Project no. TREN/07/FP6AE/S07.71574/037180 IFLY

iFly

Safety, Complexity and Responsibility based design and
validation of highly automated Air Traffic Management

Specific Targeted Research Projects (STREP)

Thematic Priority 1.3.1.4.g Aeronautics and Space

iFly Deliverable D3.2
Report on timely prediction of complex conditions for en-route aircraft

Version: Final (1.2)

M. Prandini (PoliMi), **L. Piroddi** (PoliMi), **S. Puechmorel** (ENAC), **P. Cásek** (HNWL), **S.L. Brázdilová** (HNWL)

Due date of deliverable: 22 April 2010
Actual submission date: 16 May 2011

Start date of project: 22 May 2007 Duration: 51 months

Project co-funded by the European Commission within the Sixth Framework Programme (2002-2006)		
Dissemination Level		
PU	Public	X
PP	Restricted to other programme participants (including the Commission Services)	
RE	Restricted to a group specified by the consortium (including the Commission Services)	
CO	Confidential, only for members of the consortium (including the Commission Services)	

DOCUMENT CONTROL SHEET

Title of document:	*Timely prediction of complex conditions for en-route aircraft*
Authors of document:	*M. Prandini, L. Piroddi, S. Puechmorel, P. Casek, S.L. Brázdilová*
Deliverable number:	*D3.2*
Project acronym:	*iFly*
Project title:	*Safety, Complexity and Responsibility based design and validation of highly automated Air Traffic Management*
Project no.:	*TREN/07/FP6AE/S07.71574/037180 IFLY*
Instrument:	*Specific Targeted Research Projects (STREP)*
Thematic Priority:	*1.3.1.4.g Aeronautics and Space*

DOCUMENT CHANGE LOG

Version #	Issue Date	Sections affected	Relevant information
0.1	10.08.2010	all	First Draft
0.2	21.10.2010	all	Second Draft
1.0	02.11.2010	2, 5, 8	Final
1.1	15.11.2010	all	Revised Final
1.2	16.05.2011	all	Revised Final

Version 1.2		Organisation	Signature/Date
Authors	M. Prandini	PoliMi	
	L. Piroddi	PoliMi	
	S. Puechmorel	ENAC	
	P. Cásek	HNWL	
	S.L. Brázdilová	HNWL	
Internal reviewers	H. Blom	NLR	
External reviewers			

iFly, Work Package 3, D3.2
Report on timely prediction of complex conditions for en-route aircraft

May 16, 2011

Abstract

This is Deliverable 3.2 describing the work performed under task 3.2 of work package 3 of the iFly project. The objective of task 3.2 is to develop methods for timely predicting potentially complex air traffic conditions that may be over-demanding to airborne self separation. Starting from the analysis of the requirements on complexity metrics stemming from the autonomous aircraft advanced concept of operations of the iFly project, novel methods for complexity evaluation are proposed that could play an essential role within the strategic and hazards prevention phases of the air traffic management operations. In particular, complexity evaluation on a long term prediction horizon can help to identify congested areas and support strategic flight plan optimization, whereas complexity evaluation on a mid term horizon can help to identify encounter situations that are critical for distributed conflict resolution operations.

Contents

List of acronyms

A^3 Autonomous Aircraft Advanced

AFR Autonomous Flight Rules

AMFF Autonomous Mediterranean Free Flight

ASAS Airborne Separation Assistance System

ATC Air Traffic Control

ATCC Air Traffic Control Center

ATM Air Traffic Management

BM Brownian Motion

CD Conflict Detection

ConOps Concept of Operations

CR Conflict Resolution

ECAC European Civil Aviation Conference

FOC Flight Operation Centre

IPS Interacting Particle System

SSA Self Separating Airspace

RBT Reference Business Trajectory

SDCPN Stochastically and Dynamically Coloured Petri Net

SESAR Single European Sky ATM Research

SWIM System Wide Information Management

TFM Traffic Flow Management

TM Trajectory Management

TMA Terminal Maneuvering Area

1 Introduction

1.1 Description of work package 3

The objective of work package 3 is to study and develop methods for predicting air traffic conditions that may be over-demanding to the airborne self separation design. This is a crucial task for avoiding encounters that appear safe from the individual aircraft perspective, but are actually safety-critical from a global perspective. The characterization of globally safety-critical encounters can provide useful information for the trajectory management and conflict resolution operations, and can also help in identifying the potential ground support needs within the Autonomous Aircraft Advanced Concept of Operations (A^3 ConOps) developed in work package 1 of the iFly project.

Work package 3 is structured in the following two sub-work packages:

WP3.1: Comparative study of complexity metrics. In this sub-work package, we have carried out a critical survey of different metrics proposed in the literature for complexity modelling and prediction in Air Traffic Management (ATM), [58]. Most of the current complexity metrics address ground-based ATM. Though this is reasonable within the current centralized ATM system, where aircraft follow predefined routes according to some prescribed 4D flight plan, it becomes restrictive within airborne self separation ATM systems.

WP3.2: Timely predicting complex conditions. In this sub-work package, we shall study the problem of predicting complex conditions in airborne self separation and developing a appropriate complexity metrics. For work package 3 studies, no specific choice is made regarding where to use the novel methods, airborne and/or on the ground.

1.2 Objectives and activities under the sub-work package 3.2

The goal of sub-work package 3.2 is to develop approaches to complexity evaluation that can be applied to advanced autonomous aircraft ATM systems, where a part of the responsibility in maintaining the appropriate separation between aircraft is delegated to the pilots.

In particular, pilots will take over the air traffic controllers' tasks for separation assurance in Self Separating Airspace (SSA), and they will rely for this purpose on advanced tools enabled by advanced technologies for sensing, communicating, and decision making. Centralized control will assume a new role consisting in a higher level, possibly automated, supervisory function as opposed to lower level human-based control, which should allow an increase in the airspace capacity without compromising safety.

The development phase in WP3.2 is based on

- a preliminary analysis of possible applications of complexity evaluation in the A^3

ConOps developed in wok package 1 and described in Deliverable 1.3, [13], and

- the survey work in Deliverable 3.1, [58], on the approaches to complexity evaluation that have been proposed within the current human-based centralized ATM system and may be appropriate also for the foreseen automated airborne self separation.

Work is structured into two parallel streams of activities, that is

i) the further development of a promising approach to intrinsic air traffic complexity characterization described in Deliverable 3.1, with specific focus on computational aspects

ii) the introduction of innovative approaches to complexity evaluation, better tailored to the intended A^3 ConOps applications.

The assessment phase in WP3.2 consists of evaluating the performance of the novel complexity metrics when used for identifying those air traffic configurations that are more difficult to control in a decentralized way. Experiments are performed on the hypothetical Autonomous Mediterranean Free Flight (AMFF) air traffic scenario considered in [7] for collision risk estimation by the Interacting Particle System (IPS) method.

1.3 Organization of Deliverable 3.2

Deliverable 3.2 is structured as follows. In Chapter 2, the requirements on complexity metrics stemming from the A^3 ConOps are specified based on the formalization of the A^3 ConOps in Deliverable 1.3, [13]. Chapter 3 describes the main complexity metrics proposed in the literature and discusses their drawbacks based on the characteristics that a complexity metric should possess to be applicable to airborne self separation. Chapter 4 presents further developments of a metric proposed in the literature that was first identified as possibly applicable to airborne self separation in Chapter 3. Critical aspects that hamper its use for the intended A^3 ConOps applications are pointed out. Two novel methods for complexity evaluations are then presented in Chapter 5. Their features are summarized and their performance is compared through a correlation analysis with collision risk. Finally, Chapter 6 draw concluding remarks on the achievements under WP3.2 and discusses possible further developments.

2 Possible applications of complexity metrics within the A^3 ConOps

2.1 Introduction

The A^3 ConOps described in Deliverable 1.3 of the iFly project, [13], addresses a quite challenging approach to ATM, where a net-centric environment is envisaged in which all aircraft are responsible for airborne self separation, without ground support from Air Traffic Control (ATC), while meeting traffic flow constraints. The focus is on the en-route part of the flight, with self separation capable aircraft flying in the SSA.

Trajectory-based operations are adopted to enhance the strategic ATM operations and are allowed by the dynamical sharing of the Reference Business Trajectory (RBT) to reduce uncertainty in the predicted aircraft position during its flight. The sharing of RBT information is enabled by the System Wide Information Management (SWIM) system, which incorporates ground infrastructure and air-ground data links network. As a result, the ATM focus is shifted from tactical interventions to management of RBTs which are then flown using the advanced functions of airborne systems. Nevertheless, the need for tactical ATM is still be present due to the stochastic nature of air traffic environment and the occurrence of unforeseen events.

The responsibility for tactical ATM actions is delegated to aircrew supported by airborne systems (so called Airborne Separation Assistance Systems (ASASs)). This allows more effective tactical maneuvering, since ATM actions will then be taken based on a better knowledge of the local situation which would be available onboard of the maneuvering aircraft. Nowadays, a commonly equipped aircraft with onboard sensors has better information about local environment than the air traffic controllers. In addition, the issue of getting reliable and complete information on the traffic surrounding the aircraft will be solved by progressive implementation of data link technologies, such as Automatic Dependent Surveillance - Broadcast (ADS-B) or Traffic Information Service - Broadcast (TIS-B), together with SWIM.

During the SSA part of the flight, which may consist of the whole phase between the departure and destination Terminal Maneuvering Areas (TMAs), the self separation capable aircraft can fly according to the Autonomous Flight Rules (AFR), i.e., they are responsible for the ATM separation from other traffic and obstacles (e.g., weather hazards or restricted areas).

An A^3 equipped aircraft flying through the SSA has two main objectives:

- *Performance*, considering:
  - Global ATM safety and effectiveness which is expressed in terms of various strategic (flow) constraints.
  - Own flight effectiveness reflected through different levels of trajectory and maneuver optimization.

- Own aircraft *safety* ensured by conflicts and hazards avoidance systems.

In high density airspace, the achievements of these objectives is hampered by the presence of other aircraft flying in the SSA. More specifically,

- Performance is deteriorated when the aircraft is flying through an area with highly congested traffic, since many tactical maneuvers are typically required;
- Safety might be compromised when an aircraft is involved in a safety-critical encounter situation that exceeds the capabilities of the Conflict Resolution (CR) system (automated and/or human-based).

In this context, complexity prediction and assessment play an essential role within the strategic and tactical phases of the ATM processes. Measuring air traffic complexity would serve the twofold purpose of avoiding the overload of tactical ATM (safety aspects) and the need for excessive tactical maneuvering (performance aspects).

2.2 Intended applications

Within the A^3 ConOps, two potential applications for the traffic complexity prediction can be identified. These applications and the related requirements on complexity metrics are detailed in Sections 2.2.1 and 2.2.2. One is related to the strategic trajectory planning. The other is oriented mainly to tactical actions and focused on onboard separation management.

2.2.1 Trajectory management

The primary goal of A^3 Trajectory Management (TM) is the effectiveness of the aircraft flight within a long term time horizon of more than 30 minutes, potentially for the whole autonomous part of the flight. Onboard TM considers the strategic flow management constraints (in particular, the SSA exit conditions) and the areas-to-avoid (e.g. restricted areas). In the A^3 ConOps, areas-to-avoid include also complex or congested regions.

Implementing onboard the complexity/congestion prediction system for TM would be highly ineffective. As a matter of fact, while an aircraft can obtain very accurate information on its local environment through onboard sensors and air-air data links, the additional information needed for strategic planning can only be obtained from the SWIM ground system, which would require a transmission of a huge amount of data. In view of this consideration and also of the limited computational power available onboard, it is assumed that the complexity/congestion prediction functionality involving computationally demanding tasks will be delegated to ground systems and implemented in the form of a ground automation tool. More specifically, the actual RBTs available via SWIM will be used to generate 4D (space cross time) complexity maps for different (both distributed and centralized) tools.

A schematic overview of potential applications to TM and the related communication channels is shown in Figure 1. They include the following services:

- Areas with complexity higher than a predefined threshold are sent to aircraft and used as additional information for onboard trajectory optimization.
- Complexity maps are used for a ground-based trajectory optimization (e.g., in Flight Operating Centers) and the suggested trajectory changes are sent to aircraft.
- Complexity maps are used for a ground-based centralized flow management and the corresponding flow or trajectory constraints are sent to all involved aircraft.

As the information from the ground-based complexity prediction application may be used by various users – such as different ASASs, aircrews, but potentially also by ground-based ATM systems –, the related complexity metric should not focus on one particular long term conflict resolution system.

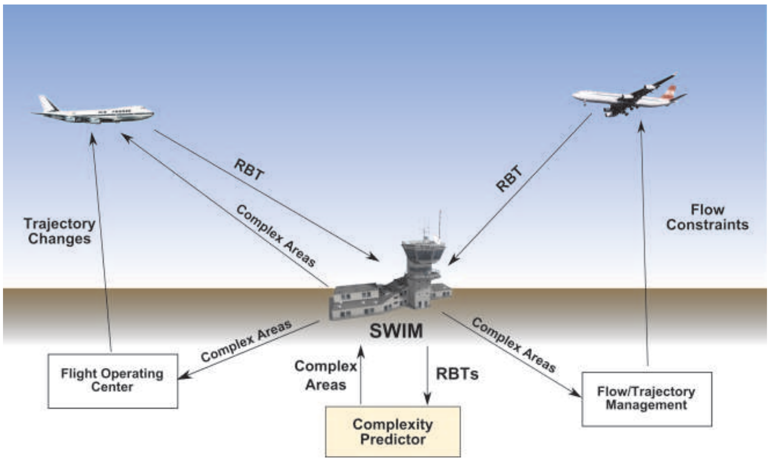

Figure 1: Potential trajectory management applications and communication overview.

As for the onboard TM application, in particular, since ground-based complexity prediction is based on the long term RBT that may undergo many changes, the resulting areas-to-avoid should be considered more as indications to the aircraft crew, not as a hard guidance for trajectory modifications. Operational validation of the concept should provide information for an effective implementation of this service.

2.2.2 ASAS mid term conflict detection and resolution

The primary goal of the ASAS mid term Conflict Detection (CD) module is the detection of hazards based on the mid term (up to 10-15 minutes) trajectories constructed from the intent messages provided by all aircraft. In addition to potential conflicts, hazards include situations that could overload the ASAS CR module. The CD function thus performs also a complexity prediction within the mid term frame and eventually issues an alert, even in absence of an aircraft conflict.

By integrating complexity evaluation within the CR module, the conflict solver could favor those resolution maneuvers with lower complexity so as to avoid further alerting and contribute to the reduction of the overall traffic complexity.

An important aspect of this application of complexity prediction is a tight relation with the CR algorithm. Complexity should mainly reflect how difficult it is for CR algorithm to solve a potential problem (in terms of number of possible solutions, complexity and effectiveness of the proposed trajectory modifications, etc.).

The concept of preservation of manoeuvring flexibility, introduced by NASA in [42, 65] and briefly revised in Deliverable 3.1 [58], represents one possible approach to this problem.

2.3 Relevant features of a complexity metric

In general terms, air traffic complexity is a concept introduced to measure the difficulty and effort required to safely manage air traffic. In the current ground-based ATM system where the airspace is structured into sectors and a team of air traffic controllers is in charge of guaranteeing safety in each sector, complexity is ultimately related to the workload, i.e., the effort exerted by humans in managing air traffic. Complexity measures are currently employed to redistribute and reassign human resources and to reconfigure sectors in order to adapt the capacity of the ATM system to the air traffic demand.

The structure and functioning of the A^3 ConOps, as well as the envisaged airborne self separation applications described in Section 2.2, pose novel requirements to complexity metrics, which ultimately result in certain key features that the metrics should possess. A list with a brief explanation of these features is reported next.

Accounting for traffic dynamics

Traffic density is the one most important factor determining the complexity of air traffic, irrespectively of the specific application. It is probably the most often considered factor and the term “congested area” is usually used to identify areas with a high traffic density. However, traffic density alone conveys only a partial information on complexity. This has been already acknowledged in the context of ground-based ATM, where it has been noted that, in certain circumstances, controllers accept traffic beyond the prescribed threshold, while in other cases they reject it despite the number of aircraft being well below the threshold, [1]. The dynamics of the traffic plays a major role in this. For example, the two patterns in Figure 2 involve the same number of aircraft at the same initial positions, but the different dynamics lead to a coherent and organized traffic flow in one case and to a chaotic situation in the other one. In the current ATM perspective, an ordered traffic flow is generally considered a low complexity situation, regardless of the number of aircraft involved, whereas only a relatively low number of aircraft is considered acceptable if the traffic pattern is chaotic. It is debatable, however, that this is going to be an equally important feature in a self separation context (see, *e.g.*, the discussion in [8]). Nevertheless, it is clear that density on its own is a crude estimator of complexity and traffic dynamics must also be accounted for.

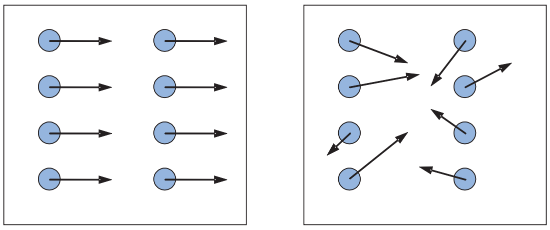

Figure 2: Different air traffic situations with the same density.

Independence of the airspace structure

In the A^3 ConOps, SSA is a sector-free context where aircraft are allowed to select their preferential routes subject to some constraints. As such, complexity metrics should not present any structural dependence on the sector characteristics. Given that the traffic density is a relevant factor for complexity characterization, [27, 41], the identification of aircraft clusters (i.e., groups of closely spaced aircraft) can complement and accelerate complexity assessment by isolating those airspace areas where to concentrate the attention.

Aircraft clustering was originally studied in connection with the conflict resolution problem [12, 62, 26, 19, 6]. The work [12], in particular, studies conditions under which separation assurance can be delegated to the cockpit, based on the idea of clusters of conflicting aircraft. A methodology for identifying aircraft clusters is suggested in [5, 4] as a first step towards obtaining a sector-independent evaluation of airspace congestion: aircraft clusters are isolated first and then congestion is assessed based on complexity evaluation in each cluster. In some sense, aircraft clusters can play within a self separation context a role similar to sectors within the centralized human-operated ATM system.

Tailoring to the look-ahead time horizon

The time dependence aspect should be better focused, introducing approaches for air traffic complexity assessment tailored to the specific time horizon. As for the foreseen applications in the A^3 ConOps to onboard trajectory management and intent-based conflict detection and resolution, we can distinguish between a long term and a mid term look-ahead time horizon, respectively.

Complexity metrics for onboard trajectory management should be computed based on the aircraft RBT over the reference (long term) time horizon for onboard trajectory optimization, which may extend to the whole duration of the autonomous part of the flight. They should detect critical situations that would require many tactical manoeuvres to be solved along the RBT of each single aircraft, and identify highly congested regions that would require an entering aircraft too many adjustments of its RBT to pass them through. Complexity should be recomputed from time to time to take care of possible modifications of the aircraft RBTs. Unexpected deviations on a finer time scale shall be accounted for by complexity metrics tailored to a mid term time horizon. Complexity metrics for supporting the intent-based conflict detection and resolution functions should detect those situations that could overload the onboard conflict resolution module. They should be computed based on the trajectories reconstructed from the state and intent information on a mid term time horizon of $10 - 15$ minutes, possibly accounting for uncertainty in the aircraft trajectory prediction due, e.g., to the wind prediction.

Independence of the control effort

A complexity metric can be classified as *control-dependent* or *control-independent*, based on whether it accounts for the controller in place explicitly or only indirectly through its effect on the air traffic. Complexity metrics incorporating air traffic controller's workload measurements are clearly control-dependent. In principle, control-dependent metrics could be employed in an airborne self separation framework too, e.g., by incorporating some measure of the control effort involved for solving a conflict in terms of deviation from the original trajectory, computational effort, etc. This approach, however, is not feasible in practice. Consider in fact that, in the A^3 ConOps, control in the SSA is delegated to the aircraft, with pilots supported in their trajectory and separation management tasks by automated tools implementing certain optimization and conflict resolution strategies. Different levels of automation could be realized: the pilot could be provided with a set of possible options to choose from or only be informed of the decision taken by some automated system, whose characteristics would depend on the adopted optimization and resolution strategy. As a result, the A^3 ConOps controller has a decentralized time-varying structure, difficult to characterize for the purpose of control effort evaluation, and involving pilots as human-in-the-loop component, with the related problems of their workload evaluation. All this makes a control-independent measure of complexity better suited for the A^3 ConOps.

A possible way of taking into account the difficulty of managing the traffic without explicitly referring to the controller in place would be to adopt the notion of *flexibility* of the aircraft trajectory, i.e., the extent to which a trajectory can be modified without causing a conflict with neighboring aircraft or entering a forbidden airspace area. In principle, the larger is the flexibility of a trajectory, the easier is to find some resolution manoeuver to avoid the occurrence of a conflict due to some unexpected deviation of a neighboring aircraft from its planned path, irrespectively of the specific control strategy used to select the best resolution maneuver. The use of flexibility measures in an airborne self separation framework is the object of an ongoing research activity by NASA, [34, 35, 33]. The concept of flexibility is used differently depending on the time horizon. In the short/medium term, flexibility is used as a criterion to rate different conflict resolution maneuvers, so that the adopted solution is the easiest to adapt to unexpected behavior by intruder traffic. In the long term horizon, a flexibility preservation function is adopted to plan the aircraft trajectory by minimizing its exposure to disturbances such as weather cells and dense traffic areas.

These two notions tailored to different look-ahead time horizons appear well-suited for the two applications to onboard trajectory management and intent-based conflict detection and resolution, the only issue being related to the lack of an effective procedure for their computation in a general 3D setting.

Goal-oriented output form

Air traffic complexity is both a time- and space-dependent feature, that is typically expressed in aggregate form by condensing either the space or the time information (or both) of the traffic situation under consideration. Output forms range from a scalar value, describing the traffic complexity in a certain region at a specific time instant, to a spatial complexity map.

Regarding the perspective applications, scalar-valued metrics (possibly projected over some look-ahead time horizon) could be better suited to the mid term conflict detection and resolution function, providing a synthetic information on the level of complexity encountered by the aircraft along its current trajectory, which should be easier to interpret. On the other hand, complexity maps can be used to identify critical areas of the airspace that the aircraft should better avoid, and, hence, are more suitable for the long term trajectory management task.

Sustainable computational load

The computational effort involved in complexity evaluation is a critical feature for ATM operations, especially in on-board applications.

It is important to note that the effort is related to the output form: those approaches providing a complexity map are typically computationally more intensive than those computing a scalar value of complexity, and for the them the memory requirements and the need for an efficient (compact and easy to interpret) representation of the information are an issue. As the computational resources available on the ground are higher than those available onboard, in the A^3 ConOps, the complexity/congestion prediction functionality for trajectory management will be implemented in the form of a ground automation tool and only relevant information on the ares-to-avoid will be uploaded to the airborne system.

A property that can reduce the computational load in trajectory management operations is that each aircraft contribution to complexity can be computed separately and then combined with that of the other aircraft to provide the overall air traffic complexity. This property in fact allows a simple evaluation of the impact of possible trajectory changes by removing the original contribution of the aircraft and replacing it with the new one based on the updated trajectory.

3 Analysis of the existing approaches to complexity evaluation in view of the A^3 ConOps application

In this Chapter 2, we evaluate the suitability and portability of existing complexity metrics to airborne self separation. A journal version of this chapter has been accepted for publication, [59].

Most of the complexity measures that have been to some extent successful within the current human-based centralized ATM system will actually turn out to be inappropriate within the A^3 ConOps, and this motivates our work on the development of novel metrics to meet the new challenges posed by airborne self separation.

3.1 Main approaches proposed in the literature

Several metrics have been proposed in the literature for the characterization of air traffic complexity. A description of selected metrics is provided next. This description is taken from Deliverable 3.1, [58]. The reader can refer to the comprehensive literature review [27] and the technical report [51] for more details on those complexity metrics explicitly accounting for the air traffic controllers' workload.

Aircraft density (AD)

In the current practice, complexity of air traffic is accounted for in terms of number of aircraft and on a per-sector basis, [66, 27]. The number of aircraft in a sector is the air traffic characteristic that has been most cited, studied, and evaluated in terms of its influence on workload. In the United States, the peak aircraft count (the largest number of aircraft in a sector during any minute of a 15 minutes time interval) is compared with an acceptable peak traffic count value, and adopted for operational traffic flow management decisions like re-routing flights out of an overloaded sector, [50]. Similarly, the European flow management staff determines the airspace configuration schedule (successive aircraft configurations during the day) by splitting or merging sectors based on the number of air traffic controllers on duty and the traffic load assessed by means of flight counts and sector capacities. A decision support system for traffic management (the Enhanced Traffic Management System) is used for this purpose, whose monitor/alert function is based on a comparison of the prediction of traffic volume in the sector against some established threshold volume representing the maximum number of aircraft that the air traffic controllers are willing to accept in that sector.

Dynamic density (DD)

Researchers unanimously agree that air traffic indicators other than the number of aircraft per sector are relevant to the air traffic controller's workload. These indicators are related to both structural and flow characteristics of air traffic, [51, 27]. The former characteristics are fixed for a sector and given by spatial and physical attributes such as terrain configuration, number of airways, airway crossings and navigation aids (*static air traffic characteristics*). The latter vary as a function of time and depend on features such as number of aircraft, weather, aircraft separation, closing rates, aircraft speeds, mix of aircraft and flow restrictions (*dynamic air traffic characteristics*). These static and dynamic factors interact in a nonlinear complex way to produce air traffic complexity, [2, 48, 10]. A list of "complexity factors" is provided in the literature review [27].

DD is an aggregate measure of complexity where traffic density and other dynamic traffic characteristics are combined linearly or through a neural network, [36, 43, 66, 39, 28, 40, 49, 50]. The characteristics are identified as critical for realtime decision making through interviews to qualified air traffic controllers and include such variables as the number of aircraft undergoing trajectory changes or requiring close monitoring due to reduced separation. The weights are determined based on subjective ratings obtained showing different traffic scenarios to the interviewed air traffic controllers or by regression analysis of their physical activity data. As a result, DD is a complexity measure that incorporates subjective and objective workload measurements.

Different DD measures have been proposed in the literature, depending on the complexity factors that they include. The choice of the complexity factors often relates to the specific Air Traffic Control Center (ATCC), which makes DD a sector-dependent metric. The structure of the airspace was actually identified as the second most important factor behind traffic volume [41]. Histon *et al.* [28, 29] investigated how this structure can be used to support abstractions that air traffic controllers appear to use to simplify traffic situations. A DD metric that includes a structural term based on the relationship between aircraft headings and the dominant geometric axis in a sector was proposed in [36]. Also, specific emphasis was given to the traffic and airspace characteristics that impact the cognitive and physical demands placed on the air traffic controller. The relation of DD with cognitive factors is investigated in [27].

Interval complexity (IC)

IC is a time-smoothed version of a DD-like measure that has been introduced in [24] as an estimate of the air traffic controller's workload in a sector.

The IC of a sector is defined as the average over a 5 to 10 minutes time window of the linear combination of the following complexity factors: number of aircraft flying within the sector, number of aircraft flying on nonlevel segments, and number of aircraft flying close to the border of the sector. Nonlevel flights and flights close to the boundary in fact require special attention and procedures to be followed by the air traffic controller. The weights in the linear combination depend on the specific sector.

Fractal dimension (FD)

FD is an aggregate metric for measuring the geometrical complexity of a traffic pattern, by evaluating the number of degrees of freedom used in the airspace by the existing air routes, [52]. This information is independent of sectorization and does not scale with traffic volume. Currently, aircraft cruise on linear routes at specified altitudes, corresponding to a geometrical dimension of 1. In the future, it is expected that flights will be allowed to move from these linear routes. If all of the airspace were covered by routes, the FD would be 3. However, there will still be preferred routes (due to the position of connected airports, or to wind currents, etc.), thereby decreasing the actual dimension of the route structure. Analysis of air traffic using a gas dynamics analogy also shows a relation between FD and the conflict rate (number of conflicts per hour for a given aircraft).

Input-output (IO) approach

In [45, 46, 47], air traffic complexity is defined in terms of the control effort needed to avoid the occurrence of conflicts when an additional aircraft enters the traffic. To this purpose the authors introduce an input-output system, where the air traffic within the region of the airspace under consideration is the system to be controlled, and an automatic conflict solver is the feedback controller. The input to the closed-loop system is represented by a (fictitious) additional aircraft entering the traffic, whereas the output is given by the deviation of the aircraft already present in the traffic from their original flight plans as issued by the feedback controller to safely accommodate the incoming aircraft. Optimization of the conflict resolution maneuvers is performed by means of a mixed integer programming (MIP) solver. The overall amount of corrective action needed to recover a conflict-free condition is taken as a measure of the air traffic complexity. A “complexity map” is constructed as a function of the entering position and bearing of the incoming aircraft. A scalar value can be extracted from this complexity map taking, *e.g.*, the “worst-case” value for the corrective action needed to safely accommodate the additional aircraft. Note that different measures of the control effort and different solvers could be used, and that the choice of the conflict solver has a large impact on complexity evaluation.

Intrinsic complexity metrics

Some researchers were not so inclined to acknowledge a direct cause-effect relation between complexity and workload, and also that the relationship between the two could be adequately expressed mathematically. This has led to a radically different view of the complexity issue, which aims at building metrics of the “intrinsic” complexity of the air traffic distribution in the airspace, without incorporating any measure of the air traffic controller’s workload, [15]. According to this viewpoint, complexity metrics should capture the level of disorder as well the organization structure of the air traffic distribution, irrespectively of its effect on the air traffic controller's workload.

Two classes of intrinsic complexity metrics are presented in [15], both based on the measurements of the aircraft velocities and positions. The first class consists in a geometrical approach where complexity is a function of the relative position vectors and relative velocity vectors of the aircraft. The second class describes traffic flow organization using the topological Kolmogorov entropy of a dynamical system modelling air traffic. The approach based on topological entropy was further developed in later work, [14, 19, 17], where the authors explore both linear and nonlinear system modelling of air traffic to derive topological entropy measures for air traffic complexity characterization, and, ultimately, to produce maps of local complexity to be used for the identification of critical air traffic areas.

Inspired by this work, in [37] the air traffic is represented through an interpolating velocity vector field, and complexity is evaluated based on the characteristics of the latter. Essentially, if the vector field is smooth, aircraft can follow non intersecting trajectories and the introduction of an additional aircraft causes a marginal increase in complexity. On the other hand, locations of the airspace where the vector field loses continuity correspond to critical areas. The main challenge of the approach is computing the separation boundary (between smooth field regions) in real-time.

In [63], to capture the complexity associated to a lack of organization, an air traffic situation is modelled by an evolution equation, with the aircraft trajectories interpreted as integral lines of some dynamical system. The Lyapunov exponents (LEs) of the dynamical system provide an indicator of the air traffic complexity, allowing for the identification of different organizational structures of the aircraft speed vectors such as translation, rotation, divergence, convergence, or a mix of them. For systems described by nonlinear differential equations, LEs measure the rate of exponential convergence or divergence of nearby trajectories, and can be taken as indicators of the level of order/disorder of a system. The idea is that the larger is a positive Lyapunov exponent, the higher is the rate at which one loses the ability to predict the system behavior. Areas characterized by high air traffic complexity are then easily identified by plotting the largest Lyapunov exponent as a function of the airspace position, thus obtaining a complexity map over the considered airspace area.

3.2 Classification of the reviewed complexity metrics

In this section we classify the approaches reviewed in Section 3.1 with respect to the features that are relevant to airborne self separation described in Section 2.3. A schematic view of this classification is reported in Table 1.

As for the "computational load" feature, only a qualitative classification of the approaches is presented. A comparison of the different approaches in terms of computational effort is quite a challenging task. Indeed, different implementations of the same approach may result in a different assessment of the computational load. Also, the comparison is fair only when made between approaches providing the same output form (a scalar value rather than a map).

As discussed before, those complexity metrics where workload and air traffic measurements are incorporated within a single aggregate indicator are control-dependent. Also, they depend on the adopted notion and measure of workload, and inherently incorporate various human factors aspects. Workload-oriented metrics are sector-based (in [24], reference is even directly made to complexity of a sector as an estimate of the air traffic controllers' workload of that sector), and often show structural dependence on the sector characteristics, which further limits their applicability to a sector-free context such as the A^3 ConOps.

AD is both a workload-dependent and sector-based metric, since it is given by the number of aircraft in a sector, which is compared with a threshold determined based on the capabilities of air traffic controllers to safely handle air traffic in that sector. Even within a ground-based ATM context, AD presents some drawbacks since it does not not take into account a few aspects that may greatly influence the actual workload levels experienced by air traffic controllers. This includes factors such as traffic pattern, traffic mix, weather, etc., the time variability of the traffic volume (a traffic volume that highly fluctuates over time is more likely to generate conflicts and appears more complex to the controller than a uniform traffic flow, [23]), and the duration of a high workload period. In turn, AD is very sensitive to the entry and exit times of a few flights which would actually not change the amount of sustained workload. Finally, human factors are also neglected, although operational errors are more likely to occur *after* rather than during a peak in traffic count [64].
Despite all these drawbacks, AD is currently considered the best available indicator of complexity in view of the simplicity of its calculation, which does not require other information than aircraft count, and of its operational interpretation, since to reduce complexity one should just limit the number of aircraft entering the sector.

The DD and IC metrics are also workload-oriented and sector-based, and are even more critically dependent on the workload evaluation method and the sector characteristics. They are in fact parametric models where different complexity factors in a sector are combined linearly or through a neural network with coefficients finely tuned based on a quantitative evaluation of the perceived workload in that specific sector. The computed weights are extremely variable from sector to sector and therefore need to be re-estimated and re-validated for each sector (and possibly periodically re-tuned). Once the weights have been set, evaluating the DD is not a computationally demanding task. From an operational viewpoint, having too many complexity factors to analyze makes it difficult for decision makers to understand which specific complexity factor is responsible for a high-workload situation and, hence, to decide what action to take to reduce complexity, [50].

The IO approach provides another control-dependent measure of complexity, which is evaluated in terms of the control effort needed to safely accommodate a fictitious additional aircraft, but avoids the workload issue by using a specific centralized conflict solver in place of the air traffic controller. A similar approach could actually be adopted

Table 1: Classification of the reviewed complexity metrics.

metric	**input data**	**method**	**accounting for traffic dynamics**	**sector-independent**	**look-ahead time horizon**	**control-independent**	**output form**	**computational load**
Aircraft density	number of aircraft in the sector	comparison with a workload-based threshold	no	no (evaluated per sector)	instantaneous measure, extendable with trajectory prediction	no (threshold tuned on workload)	scalar value	small
Dynamic density	number of aircraft and other indicators of traffic characteristics in the sector	linear and non-linear regression tuned on workload data	yes (through synthetic indices)	no (tuned to the specific sector)	instantaneous measure, extendable with trajectory prediction	no (regression weights tuned on workload)	scalar value	significant when defining the relative weights, small in the on-line usage
Interval complexity	number of aircraft and other indicators of traffic characteristics in the sector over a 5 to 10 minutes horizon	linear and non-linear regression tuned on workload data, plus averaging	yes (through synthetic indices)	no (tuned to the specific sector)	short/mid term	no (regression weights tuned on workload)	scalar value	significant when defining the relative weights, medium in the on-line usage (trajectory prediction is needed)
Fractal dimension	aircraft trajectories	covering measure	yes	yes	long term	yes	scalar value	significant
Input/output approach	aircraft timed trajectories	optimization of conflict resolution maneuvers for all possible initial conditions of an additional aircraft	yes (indirectly through trajectory changes to accommodate a new aircraft)	yes	short/mid term	no (based on control effort evaluation)	map (control effort to accommodate an additional aircraft as a function of its initial conditions)	high
Lyapunov exponents	aircraft timed trajectories	dynamical systems modelling of trajectories and calculation of Lyapunov exponents	yes	yes	short/mid/long term	yes	map (largest Lyapunov exponent as a function of airspace position)	high

for tuning the coefficients in the DD and IC aggregate complexity metrics, replacing the air traffic controller with some conflict solver. As for the computational effort involved in the IO map computation, it depends on the adopted conflict solver. Some gridding procedure has to be adopted to build the map.

Note that all the DD, IC, and IO control-dependent metrics could, in principle, be adapted to airborne self separation, by substituting the evaluation of the control effort with that of the trajectory flexibility, as suggested in Section 2.3 when discussing the "independence of the control effort" feature.

The control-independent FD and LE metrics appear to be more directly applicable to the A^3 ConOps. In fact, since they depend only on the air traffic characteristics, they can be used to evaluate both uncontrolled and controlled aircraft trajectories, and in the latter case they do not require the knowledge of the controller in place, which is accounted for only indirectly, through the effect of its action on the air traffic organization.

Regarding the time dependence aspect, those measures that are computed based on the aircraft future trajectories (such as FD, IO, and LE) are naturally evaluating complexity over some look-ahead time horizon. As for FD, in particular, it can be thought as a geometrical feature of a limit shape obtained by observing trajectories on an infinite time period. As such it is a complexity metric potentially suitable for long term applications. Unfortunately, it has a great drawback that limits its operational impact, in that the timing information of the aircraft routes is completely lost in this type of analysis. It was in fact originally proposed as a measure to compare traffic configurations resulting from various operational concepts, [52], with the key feature of allowing to decouple the complexity due to airspace partitioning in sectors from the complexity due to traffic flow features, and of being independent of workload aspects.

Those measures that are computed based on the air traffic state rather than the whole aircraft trajectories can be used to predict complexity in the future when combined with trajectory prediction (by projecting the air traffic state and recomputing the complexity measure). In [66], it is in fact suggested that DD can be projected over a suitable time horizon by using trajectory prediction tools, so as to forecast future workload levels and use this information for traffic management purposes. Good prediction accuracy is reported in the 5 minutes scale, suitable for short term control applications. Extension of the prediction horizon to 20 minutes could be of use for mid term control applications. The projection of the IC metric on a further extended time scale of 20 to 90 minutes could be used for selecting appropriate "complexity resolution" actions minimizing and balancing traffic complexities between adjacent sectors of a certain airspace region.
Note that the reliability of the complexity prediction on some look-ahead time horizon depends anyway on that of the aircraft trajectories prediction. Surprisingly, to our knowledge, uncertainty in the trajectory prediction is not accounted for in any of the (deterministic) approaches presented in the literature.

Regarding the output form, AD, DD, IC, and FD are all scalar metrics, but only AD, DD, and IC are extendable in time through aircraft trajectories prediction. The output of the IO method is a map of the control effort as a function of the initial conditions of an hypothetical additional aircraft entering the considered airspace region. As such, this map provides only indirect information on the spatial distribution of complexity in the airspace, which hampers its use for the identification of complex areas-to-avoid. On the other hand, the spatial complexity maps derived based on LEs could support decision making in the trajectory management function by isolating critical areas.

LE presents the drawback of being computationally demanding. More specifically, the main challenge from a computational viewpoint is represented by the calculation of the vector field that smoothly interpolates a given set of aircraft positions and velocities.

3.3 Concluding remarks

In this chapter, requirements posed by the A^3 ConOps applications on complexity metrics have been discussed, and existing metrics have been critically revised, discussing their portability and adaptability to the new airborne self separation context. In particular, the elusive notion of control effort, that is generally incorporated in the complexity measure, has been found to be one of the main obstacles towards a definition of reliable complexity indicators. The only metrics that appear portable to the A^3 context are the so-called "intrinsic metrics" and, in particular, the one based on the Lyapunov exponents of the dynamical system that describes the air traffic evolution. Computationally more effective procedures to determine the dynamical system matching the air traffic should be conceived to make it applicable within the A^3 ConOps. This has been part of the work performed in WP3 and is documented in Chapter 4. Further novel approaches have been developed in parallel to meet the challenges posed by the A^3 applications. These approaches are described and analyzed in Chapter 5.

4 The Lyapunov exponents based method for complexity evaluation

In this chapter, we describe in some detail the approach to complexity evaluation based on Lyapunov exponents developed in [16, 17, 19]. This approach has been identified in Chapter 3 as the more promising for application to the A^3 ConOps among the approaches proposed in the literature. One of its key features is that complexity is evaluated without making reference to the way the traffic is controlled (that is human controller, full automated control or some hybrid approach) but considering the trajectories of aircraft as observations of an underlying hypothetical flow whose geometrical properties define complexity. Our goal in this chapter is to shed light on the computational challenges of complexity computation and describe possible ways to speed up the approach. We also clarify at the end of the chapter which are the limits of the approach with respect to the envisaged A^3 ConOps applications.

4.1 Some basic complexity indicators

The first intrinsic indicator of complexity that can be considered is a simple extension of the number of aircraft in a sector, but designed so that no reference is made to the airspace structure. It is in some sense a local density indicator. Let $w\colon \mathbb{R} \to \mathbb{R}^+$ be a smooth rapidly decreasing function and let $(x_j)_{j=1\ldots N}$ be a traffic sample with x_i corresponding to position of aircraft i. The local density around a point $x \in \mathbb{R}^3$ will be defined as:

$$D(x) = \sum_{j=1}^{N} w(\|x - x_j\|).$$

One can compute the integral of D over the entire space to obtain an aggregate value for the density:

$$I = \int_{\mathbb{R}^3} D(x)dx = \sum_{j=1}^{N} \int_{\mathbb{R}^3} w(\|x - x_j\|)dx = N \int_{\mathbb{R}^3} w(\|x\|)dx.$$

If the integral of the window function w over the entire space is 1, then the integral of the local density is simply the number of aircraft. It has to be noted that the definition of local density is in some sense isotropic: $D(x)$ is a sum of radial basis function (i.e., functions depending only on a norm). Some freedom remains in the choice of the norm, that allow to take into account for example the difference between vertical and lateral separations for aircraft. The local density has minimum possible value 0 (this can occur with compactly supported w and points far away all aircraft). The maximum value of $D(x)$ is of course dependent on the shape of the window function; however, it is classical to take $w(0) = 1$ and let the value decrease to 0 as the argument is going to $+\infty$. In this case, the value of D tend to N when all aircraft are located near a single point. Most of the time, local density is computed on a regular grid, that is used to produce a complexity map of the traffic. This can be very time consuming for large airspaces since except for the case of compactly supported w, the algorithmic complexity for evaluating the local density at a point is of order $O(N)$ with N the number of aircraft. A simple trick allows a very fast computation in the case of evaluation on the points scattered on a regular grid. First, let w be a window function (for the sake of simplicity, it is assumed smooth and rapidly decreasing, but this is not mandatory) and let $W\colon x \mapsto w(\|x\|)$ the associated radial basis function. The Fourier transform $\widehat{W}$ of W is:

$$\widehat{W}(\xi) = \int_{\mathbb{R}^3} w(\|x\|) e^{-i\langle x,\xi\rangle} dx.$$

By a polar change of coordinates we have:

$$\widehat{W}(\xi) = \int_{\mathbb{R}^+} \int_{\mathcal{S}_2} r^2 w(r) e^{-ir\langle\sigma,\xi\rangle} d\sigma dr$$

with $\mathcal{S}_2$ the unit sphere in $\mathbb{R}^3$, $d\sigma$ the solid angle measure on it. Since $d\sigma$ is a rotation invariant measure, it is possible to take ξ as defining the polar axis of $\mathcal{S}_2$, yielding:

$$\widehat{W}(\xi) = \int_{\mathbb{R}^+} \int_{[0,2\pi]} \int_{[-\frac{\pi}{2},\frac{\pi}{2}]} w(r) r^2 e^{-ir\|\xi\|\sin\phi} \cos\phi \, d\phi \, d\theta \, dr.$$

Since there is no dependance in θ, the integral reduces to the simple form:

$$\widehat{W}(\xi) = 4\pi \int_{\mathbb{R}^+} r \frac{\sin(r\|\xi\|)}{\|\xi\|} w(r) dr$$

proving that $\widehat{W}$ is again a radial basis function. The Fourier transform of D computes as:

$$\widehat{D}(\xi) = \widehat{W}(\|\xi\|) \sum_{j=1}^{N} e^{-i\langle x_j,\xi\rangle}.$$

At a first sight, it seems that noting has been gained by switching to Fourier transform except that the summation is now a little bit easier since it involves only trigonometric functions that evaluate quickly on most modern computing architectures. Nevertheless, it exists a fast algorithm for computing sums like:

$$\sum_{j=1}^{N} e^{-i\langle x_j,\xi\rangle}$$

for ξ scattered on a regular grid: the Lomb periodogram. First of all, we have:

$$e^{-i\langle x_j,\xi\rangle} = exp(-ix_{1j}\xi_1) exp(-ix_{2j}\xi_2) exp(-ix_{3j}\xi_3) \tag{1}$$

with $x_j = (x_{1j}, x_{2j}, x_{2j})$ and $\xi = (\xi_1, \xi_2, \xi_3)$. The trigonometric function being smooth, it is possible to find a local approximation of the one dimensional terms involved in (1) by a sum of terms computed on a regular grid of size P with step h:

$$exp(-ix_{1j}\xi_1) = \sum_{k=l_j}^{m_j} \alpha_{k,j} exp(-it_k\xi_1).$$

The points t_k are assumed to be evenly spaced (see Figure (3)) while the α_k are interpolating weights (many different kind of interpolation formulas can be used to obtain them: polynomial interpolation is very common).

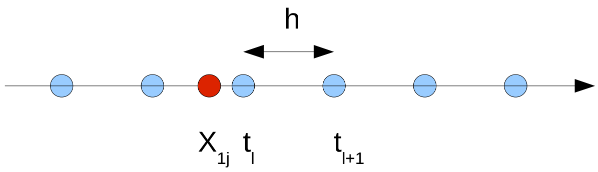

Figure 3: Local interpolation

The computation of a 1-dimensional sum:

$$\sum_{j=1}^{N} exp(-ix_{1j}\xi_1)$$

can be expressed using only values on a regular grid as:

$$\sum_{k=1}^{P} exp(-it_k\xi_1)q_k \tag{2}$$

with:

$$q_k = \sum_{j=1}^{N} \alpha_{k,j}$$

(the interpolation weights are assumed to be 0 outside the interval $[l_j, m_j]$). Looking at (2), it appears to be a discrete Fourier transform of the sequence $(q_k)_{k=1...P}$. If we seek at computing the Fourier transform at regularly spaced ξ_1, this thus can be done very efficiently by a Fast Fourier Transform (FFT) algorithm. Furthermore, since the complete 3-dimensional sum is a sum of 1-dimensional factors, the overall algorithm complexity has the same order as the FFT alone, that is $O(N \log_2 N)$. To conclude on the algorithmic complexity, it is enough to note that the number of terms in the interpolation formula depends only on the step of the grid. The previous algorithm can be applied to any evaluation of sums of radial basis functions on a regular grid.

Local density is an intrinsic complexity metric. However, it is a purely geometrical indicator and is not related to temporal evolution of the traffic. As such it is a crude estimator of the complexity: it is only a simple extension of the operational congestion indicator. The organisation of the traffic is not taken into account. In many cases, it is very important to distinguish between situations depending on the future and a temporal extension has to be considered.

Some extensions of local density to take velocities into account have been designed ([16]), and allow to refine somehow the local density. Some of these estimators will not fall within the scope of applicability of the fast algorithm, thus limiting their usefulness to small airspaces.

Assuming that the trajectory of aircraft i is given by the mapping $\beta_i\colon [a,b] \to \mathbb{R}^3$, the local density as a function of time is:

$$D(x,t) = \sum_{i=1}^{N} W(\|x - \beta_i(t)\|)$$

Given an x, the time derivative is thus:

$$\frac{\partial D}{\partial t}(x,t) = \sum_{i=1}^{N} \frac{\langle \dot{\beta_i(t)}, \beta_i(t) - x\rangle}{\|x - \beta_i(t)\|} W'(\|x - \beta_i(t)\|)$$

It can be recognized that the previous expression has the form of the so-called optical flow equation. This induces in representing the traffic as the flow of a vector field, thus interpolating between sample points. A very basic way of doing that is by assuming that the interpolating vector field is linear. It is very easy to find, by standard linear least squares, a matrix A and a vector v such that the velocity field is given by $X(x,t) = Ax + v$ and that best interpolates the observations, that is X is such that:

$$\sum_{i=1}^{N} \|v_i - Ax_i - v\|^2$$

is minimum (we recall that v_i is the observed velocity at sample point x_i). In order to obtain a meaningful picture of the complexity, such a linear model can be used only by considering aircraft close to a given point. The local behavior of the traffic can be recovered using the eigenvalues of the matrix A. A summary is given in Figure 4.

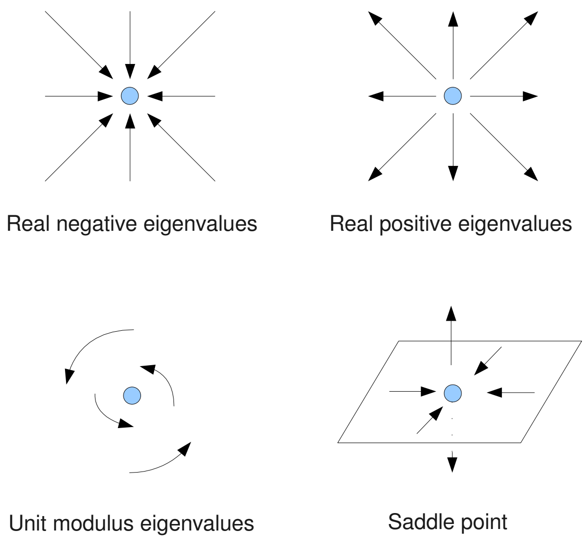

Figure 4: Geometrical view of Lyapunov exponents

4.2 A local picture of evolution: the Lyapunov exponents

The generalization of local behavior for linear system can be done by introducing Lyapunov exponents that can be interpreted as shear factors. As before, we assume that a velocity field X is defined on a domain $\mathcal{S}$. Given an initial position x_0 at time $t = 0$, we defined the flow $\beta(t, x_0)$ as the solution of the equation:

$$\frac{d}{dt}\beta(t, x_0) = X(\beta(t, x_0))$$

with condition $\beta(0, x_0) = x_0$. If now $t \mapsto \beta(t, x_0) + \epsilon(t)$ is a nearby trajectory, the variational equation for flow gives an order one approximation for ϵ as the solution of:

$$\frac{d}{dt}\epsilon(t) = X'(\beta(t, x_0))\epsilon(t)$$

so that the perturbation ϵ obeys (approximately) a linear but time dependent equation. Given an initial $\epsilon(0) = v$, the forward Lyapunov exponent at x_0 and direction v is:

$$\lambda^+(v) = \limsup_{t \to +\infty} \frac{1}{t} \log \|\epsilon(t)\|$$

Intuitively, Lyapunov exponents will find a "mean" exponential behavior for perturbation around a nominal trajectory: when the exponents are positive (resp. negative), nearby trajectories tend to diverge (resp. converge) exponentially fast.

It seems at first sight that one can obtain as many different exponents as initial direction: it turns out that in fact only a finite number of these exponents can be generated by varying v. To see that, note that since the equation satisfied by ϵ is linear, any linear combination of two solutions is again a solution. Thus we have for any real number α:

$$\lambda^+(\alpha v) = \lambda^+(v)$$

and, for any two initial conditions u, v:

$$\lambda^+(u + v) \leq \max(\lambda^+(u), \lambda^+(v))$$

(this last equation is obtained from the fact that if ϵ_1, ϵ_2 are solution of the differential equation with respective initial conditions u, v, then $\epsilon_1 + \epsilon_2$ is the solution with initial condition $u + v$ and the proposition follows from $\|\epsilon_1(t) + \epsilon_2(t)\| \leq 2\max(\|\epsilon_1(t)\|, \|\epsilon_2(t)\|)$). In fact we have more: since $u = u + v - v$:

$$\lambda^+(u) \leq \max(\lambda^+(u + v), \lambda^+(v))$$

Assuming that $\lambda^+(v) < \lambda^+(u)$ then it comes:

$$\lambda^+(u + v) \geq \max(\lambda^+(u), \lambda^+(v))$$

Since u, v play symmetric roles:

$$\lambda^+(u + v) = \max(\lambda^+(u), \lambda^+(v))$$

This important result implies in turn that if for two non zero u, v, $\lambda^+(u) \neq \lambda^+(v)$ then u, v are linearly independent. Take for example $\lambda^+(u) < \lambda^+(v)$ and $\alpha_1 u + \alpha_2 v = 0$. Applying the previous results yields:

$$\lambda^+(\alpha_1 u + \alpha_2 v) = -\infty$$

$$= \max(\lambda^+(u), \lambda^+(v))$$

which is not possible for non zero u, v unless $\alpha_1 = \alpha_2 = 0$. As a consequence, it is not possible in a n-dimensional space to find more than n different Lyapunov exponents.

The definition given above for Lyapunov exponents is interesting mainly for theoretical derivations and to get a picture of what is going on. For practical computation of Lyapunov exponents, the fact that we need a $\limsup$ is not ideally suited. Fortunately, it is possible in many cases to obtain an equivalent but much more tractable formula.

Lemma 1 *Let:*

$$\frac{d}{dt}v(t) = A(t)v(t)$$

be a linear differential equation. It exists a smooth mapping $t \to Q(t)$ with values in the unitary matrices such that:

$$\frac{d}{dt}Q^{-1}(t)v(t) = T(t)Q^{-1}(t)v(t)$$

with $T(t)$ an upper triangular matrix.

Because it has some interest for our purpose, we will give an outline of the proof of the lemma. First, take $e_1, \ldots e_n$ a basis and construct the solutions $e_1(t), \ldots e_n(t)$ of the differential equation with respective initial conditions $e_1, \ldots e_n$. Let $E(t)$ be the matrix with columns $e_1(t), \ldots e_n(t)$ ($E(t)$ describes how the original basis is deformed by the flow). $E(t)$ admits a (smooth) decomposition $E(t) = Q(t)R(t)$ with $Q(t)$ unitary and $R(t)$ upper triangular with positive diagonal elements. It is clear from the definition that:

$$\frac{d}{dt}E = AE$$

so that:

$$AE = \frac{dQ}{dt}R + Q\frac{dR}{dt}$$

using the fact that Q is unitary and R is invertible:

$$T = {}^tQAQ - {}^tQ\frac{dQ}{dt} = \frac{dR}{dt}R^{-1}$$

proving that T is upper triangular as a product of two upper triangular matrices. Now, by the change of variable $y(t) = Q^{-1}(t)v(t)$, we obtain the equation:

$$\frac{d}{dt}y = ({}^tQAQ - {}^tQ\frac{dQ}{dt})y = Ty$$

which proves the lemma. In the previous representation, the diagonal elements of the matrix R are positive. It is thus possible to write this matrix as:

$$\begin{pmatrix} e^{\mu_1} & r_{12} & \ldots & r_{1n} \\ 0 & e^{\mu_2} & \ldots & r_{2n} \\ 0 & \ldots & 0 & e^{\mu_n} \end{pmatrix}$$

The matrix T involved in the lemma is equal to $\frac{dR}{dt}R^{-1}$ and can be written as:

$$\begin{pmatrix} \frac{d\mu_1}{dt} & \dots & \dots & \dots \\ 0 & \frac{d\mu_2}{dt} & \dots & \dots \\ 0 & \dots & 0 & \frac{d\mu_n}{dt} \end{pmatrix}$$

A very interesting property is that the limit:

$$\lim_{t \to +\infty} \frac{\mu_i}{t}$$

is precisely a Lyapunov exponent (and for almost all initial conditions, the sequence of Lyapunov exponents obtained by considering diagonal entries of R is in increasing order). Since we are dealing with true limits and not with $\limsup$, this formula gives a procedure for computing Lyapunov exponents. Nearly all know algorithms used for finding the Lyapunov exponents (or only the k largest) rely on the previous decomposition. Another interesting point is that the sum of the Lyapunov exponents (that is the trace of the matrix R) gives the speed of variation of the volume of an elementary parallelepipede along the flow.

Recalling that Lyapunov exponents describe the local behavior of a system, taking into account the temporal evolution, they constitute a generalization of our first geometrical indicators. For the purpose of finding an intrinsic indicator of the complexity of the traffic, Lyapunov exponents are very good candidates. As we will see later, their major drawback is the computational load required for their evaluation.

4.3 Lyapunov exponents computation

Regardless of the method used to obtain the interpolating velocity field (local linear models or dynamic splines), there is a number of numerical pitfalls when trying to compute Lyapunov exponents. As mentioned before, the method of choice is to find a QR decomposition of the matrix A obtained by transporting a basis $(e_1, \dots, e_n)$ through the flow, then relate Lyapunov exponents to diagonal entries of the matrix. It is very inefficient to estimate A and to factor it as QR time step by time step: a differential equation satisfied by Q and R is solved instead, thus producing in a single step an updated factorization. Based on the equation established before, if $X'(\beta(t))$ is the derivative of the field at time t along the trajectory β:

$${}^tQ\frac{Q}{dt} + \frac{dR}{dt}R^{-1} = {}^tQX'(\beta(t))Q$$

to simplify the notations, we put:

$$S(t) = {}^tQX'(\beta(t))Q$$

Since ${}^tQQ = Id$:

$$\frac{d^tQ}{dt}Q = -{}^tQ\frac{Q}{dt}$$

this matrix is skew-symmetric: its diagonal entries must be 0. When considering the equation of evolution for these entries only, we obtain that:

$$\lambda_i'(t) = S_{ii}(t)$$

with $\lambda_i(t)$ the i-th diagonal term of R. A simple ordinary differential equation solver can be used to find $\lambda_i(t)$ given $S_{ii}(t)$. At the same time, since $\frac{dR}{dt}R^{-1}$ us upper triangular, all the elements of $D = {}^tQ\frac{Q}{dt}$ located below the main diagonal can be identified:

$$\forall i < j, D_{ij} = S_{ij}(t)$$

Because D is skew-symmetric, all the elements of D are known. Again, a standard differential equation allows to compute $Q(t)$ as the solution of:

$$\frac{Q}{dt} = QD$$

Note that only the diagonal elements of R are useful to compute Lyapunov exponents: the remaining terms can be left unevaluated. The main concern with the algorithm given above is that Q may (and indeed will) fail to be orthogonal during the time evolution. Since this property is required, any algorithm computing Lyapunov exponents has to correct Q from time to time. An interesting alternative approach has been presented in [38]: instead of periodically orthogonalizing Q, a representation is chosen so that orthogonality of Q is guaranteed. It is well known that any rotation matrix in dimension n can be obtained as a product of $n(n-1)/2$ elementary Givens' rotations with angles $\theta_{ij}, i = 1 \ldots n, i < j$. The parametrization of Q is obtained precisely by the θ_{ij}. The details can be found in the original article. It has to been noted however that the method is interesting mainly in low dimension, which is our case ($n = 3$). This algorithm has been successfully implemented in our application.

4.4 Interpolating vector fields

4.4.1 Vector splines

As previously stated, the first step for obtaining traffic complexity is to generate a continuous (and smooth enough) vector field interpolating the observed aircraft velocities. Formally, this problem can be described as finding a mapping $X: \mathbb{R} \times \mathbb{R}^3 \to \mathbb{R}^3$ such that, given observations $(t_i, x_i, v_i)_{i=1\ldots N}$ with x_i, v_i the position and velocity at time t_i for the sample i, we have:

$$X(t_i, x_i) = v_i, \quad i = 1 \ldots N \tag{3}$$

Unfortunately, this problem is ill-posed since infinitely many vector fields X can solve it, even if high smoothness conditions are added. To obtain a tractable criterion, it is needed to add a minimality requirement based on an energy like functional. More specifically, given a differential operator L, we want to find a X that realizes the minimum of:

$$E(X) = \int_{\mathbb{R}} \int_{\mathbb{R}^3} \|LX(t,x)\|^2 dx dt$$

under the interpolation constraints (3). This is the standard framework of vector $\mathcal{L}$-splines ([3]) when the vector field X is assumed not to depend on time (the time integral in the energy functional is dropped). With some technical assumptions on X, one can show that the optimal X can be written as:

$$X \colon x \mapsto \sum_{i=1}^{N} \lambda_i^t G(x, x_i) + Q(x)$$

where λ_i is a vector coefficient in $\mathbb{R}^3$, G is the Green's function associated with the differential operator $L^t L$ and Q is an element of the null-space of $L^t L$. The vector coefficients λ_i can be identified using the interpolation condition:

$$\sum_{j=1}^{N} \lambda_j^t G(x_i, x_j) + Q(x_i) = v_i, \ \forall i = 1 \dots N. \tag{4}$$

Most of the time, Q is a polynomial and can be expressed as a sum:

$$\sum_{k_1=1}^{d_1} \sum_{k_2=1}^{d_2} \sum_{k_3=1}^{d_3} a_{k_1,k_2,k_3} x_1^{k_1} x_2^{k_2} x_3^{k_3}$$

where x_1, x_2, x_3 are the components of the vector x. Putting this in (4), we obtain a linear system in $\lambda_i, a_{k_1,k_2,k_3}$:

$$\forall i = 1 \dots N, \sum_{j=1}^{N} \lambda_j^t G(x_i, x_j) + \sum_{k_1=1}^{d_1} \sum_{k_2=1}^{d_2} \sum_{k_3=1}^{d_3} a_{k_1,k_2,k_3} x_{i,1}^{k_1} x_{i,2}^{k_2} x_{i,3}^{k_3} = v_i$$

This linear system can be solved with classical algorithms, but is it faster in most cases to use a Krylov solver as described below. Furthermore, Krylov solvers can avoid the explicit construction of the matrix based on the $G(x_i, x_j)$, which helps reducing the computer memory needed.

Krylov solvers. To find the vectors λ_i occurring in the expression of the optimal interpolating velocity field, a linear problem has to be solved as indicated in the previous section. For small airspaces, the number of observations is typically in the order of some hundreds, allowing to solve for the λ_i by using standard linear algebra algorithms, either based on normal equations or QR decomposition (preferred in our case since some traffic situations may induce rank degeneracies in the design matrix). However, when the size of the data set is increased above one thousand, the computational burden is generally too high (on a standard PC, one can expect computation times in excess of 1 hour). To address this specific issue, it is necessary to switch to an iterative approximate algorithm for which the complexity scales only in the square of the number of observations instead of the cube. The Green's function used in field expansion is a diagonal one so that a set of 3 independent scalar least square problems has to be solved instead of a vector one. In the following, we will thus assume that we want to solve:

$$\min \sum_{i=1}^{N} \|a_i - \sum_{j=1}^{N} \lambda_j \tilde{p}(x_i - x_j, t_i - t_j)\|^2$$

with $(\lambda_j)_{j=1\dots N}$ real coefficients. The most basic iterative algorithm for finding the λ_j starts with an initial guess $(\lambda_j(0))_{j=1\dots N}$ and evolve according to a fixed step gradient rule:

$$\lambda_k(n+1) = \lambda_k(n) - \mu \sum_{i=1} (\tilde{p}(x_i - x_k, t_i - t_k), e_i)$$

with:

$$e_i = a_i - \sum_{j=1}^{N} \lambda_j \tilde{p}(x_i - x_j, t_i - t_j)$$

Introducing the design matrix:

$$L_{ij} = \tilde{p}(x_i - x_j, t_i - t_j)$$

and the vectors $a = (a_1, \dots, a_N)$ and $\lambda = (\lambda_1, \dots, \lambda_N)$, the iteration can be written more compactly as:

$$\lambda(n+1) = \lambda(n) - \mu L^t r(n)$$

with:

$$r(n) = a - L\lambda(n)$$

For a sufficiently small μ, the algorithm will converge, but only at a linear rate. To increase the speed of convergence, several techniques can be applied. Krylov subspace methods have been widely used in such cases and exhibit very good behavior. Starting from the gradient iteration, we see that for a given n, $\lambda(n)$ is an element of the subspace spanned by the vector λ_0 and the vectors:

$$\begin{aligned}
&{}^tLr(0), \\
&({}^tLL)^tLr(0), \\
&\dots, \\
&({}^tLL)^{n-1t}Lr(0))
\end{aligned}$$

The subspace generated by the iterates:

$$({}^tLL)^{it}Lr(0), i = 1 \dots n-1$$

is the Krylov subspace:

$$K_n({}^tLL, {}^tLr(0))$$

The key point in Krylov subspace methods is to use this property to generate $\lambda(n)$ not by the gradient but instead by finding the vector in:

$$\lambda_0 + K_n({}^tLL, {}^tLr(0))$$

that minimize the least square criterion. This can be done easily by iteratively find an orthonormal basis of:

$$K_n({}^tLL, {}^tLr(0))$$

and project the residual $r(n-1)$ on it. As is, the algorithm performs very well on our problem: on a bench situation with 1000 aircraft and 10 observations per aircraft, the solution if found within a 1% accuracy in 2 minutes on a PC with 3.2Ghz Xeon processor. It is anyway possible to do even better by changing the Krylov subspace to:

$$K_n(L, r(0))$$

that still allows super-linear convergence but at the expense of a single matrix-vector product in each iteration. Furthermore, it is no longer needed to explicitly form the design matrix L, thus drastically reducing memory needs. With this Krylov subspace method, it is possible to address problems with 10000 aircraft and 10 observations per aircraft while keeping resolution times within the 10 minutes range.

It has to be noted that it is in principle possible to design a fully parallel algorithm on a cluster of computers.

4.4.2 Local linear models

Let $x \in \mathcal{S}$ be given. Instead of finding a global fitting vector field X, we look at the Taylor expansion of X in a neighborhood of x:

$$X(u) = X(x) + X'(x)(u-x) + o(\|u-x\|)$$

Of course $X(x)$ and $X'(x)$ are unknown since X itself is unknown, but it is possible, since the Taylor expansion (without the o term) is linear, to estimate them as the optimal solution of the least square problem:

$$\sum_{i=1}^{N} w(\|x-x_i\|)\|v_i - a - M(x_i - x)\|^2$$

with $a \in \mathbb{R}^3$ the approximation of $X(x)$ and M a square 3×3 matrix approximating $X'(x)$. w is a non negative window function of unit L^1 norm enforcing the fact that the solution is valid only in a neighborhood of x. Classical choices for w are:

- $w(t) = \frac{3}{4\pi s^3} 1_{[0,s](t)}$, $s > 0$.
- $w(t) = \frac{15}{2\pi s^5}(1-t)^2 1_{[0,s]}(t)$, $s > 0$ ("Epanechnikov").
- $w(t) = \frac{\sqrt{8\pi}}{\sigma} e^{-\frac{t^2}{2\sigma^2}}, \sigma > 0$ (Gaussian window).

The length s of the window (or the standard deviation σ in the Gaussian case) is a free parameter of the method that needs to be adjusted. When it is small, only the aircraft close to x are really significant: the vector field X tends to follow closely these observations at the expense of lower smoothness. On the other hand, high s or σ values produce very smooth fields with poor interpolation properties. One way of finding an optimal balance between the two criteria is by leave-one-out procedure (an efficient implementation exists for local linear models). An heuristic approach is possible too, a good choice being that the window has to include a fixed (between 5% and 20 %) amount of the samples: this gives in practice sufficiently good results. To obtain a closed form expression for a, M, it is convenient to define V, W to be the N-dimensional vector:

$$V = (v_1, \dots, v_N)$$

W to be the $N \times N$ diagonal matrix:

$$W = \mathrm{diag}(w(\|x - x_1\|), \dots, w(\|x - x_N\|))$$

and A the $N \times 4$ matrix:

$$A = \begin{pmatrix} 1 & x_1 - x \\ 1 & x_2 - x \\ \dots & \dots \\ 1 & x_N - x \end{pmatrix}$$

With this convention, the least square criterion can be written in a synthetic form:

$$\|W^{1/2}(V - AL)\|^2$$

where the norm is in $\mathbb{R}^N$ and L is the matrix of unknowns:

$$L = \begin{pmatrix} a \\ \hline {}^tM \end{pmatrix}$$

Solving for M can be done classically using normal equations. The optimal L has to satisfy:

$${}^tAW(V - AL) = 0$$

or, if $({}^tAAW)$ has full rank:

$$L = ({}^tAAw)^{-1t}AWV$$

The inverse of ${}^tAAW$ is never computed directly: instead, the Cholesky decomposition ${}^tZZ = {}^tAAW$ with Z lower triangular is used. It is sometimes interesting, namely to increase numerical stability, to use QR decompositions instead of solving using the previous expression. For that purpose, a reduction by orthogonal transformation is applied and yields an equivalent problem with criterion:

$$\|{}^tQW^{1/2}V - RL\|^2$$

with R a block upper triangular matrix. For large N, QR reduction involves about twice as many operations than normal equations, for an increase in numerical accuracy and stability (the interested reader is referred to [25]). In our case, speed of evaluation is more important than numerical properties. Furthermore, the matrix:

$$^{t}AAW$$

is only 4×4, so that Cholesky decomposition almost never breaks. The overall complexity for evaluating $X(x)$ scales linearly with the number of aircraft measurements. When the window function w is compactly supported, algorithmic complexity is further reduced since only a subset of the complete sample has to be included for evaluating the model at a point: if the heuristic approach is chosen, scaling is still linear with the number of samples, but the constant of proportionality is reduced.

An obvious interest of the method is that it produces also an estimate of the matrix $X'(x)$ that is of great interest for the computation of Lyapunov exponents.

4.5 Limits of the method for the A^3 ConOps application

A main drawback of the approach described in this chapter is that it is computationally demanding. The bottleneck is represented by the computation of a smooth vector field that matches the (observed or predicted) values of the aircraft velocities at the sample points.

As we have seen, this problem can be formulated as that of optimizing a functional related to the derivatives of the field under the interpolation constraint and, in the case when the field is assumed to be time independent, its solution can be expressed as a weighted sum of radial basis functions known as vector splines. The weights in the sum are determined by solving a linear system of equations, whose complexity scales as n^3 where n is the number of samples. Improvements on the computation speed have been made by using Krylov solvers. Remaining possible speed-up are more related to hardware: it seems that the code can be made parallel and run on cluster of GPUs to achieve a speed-up factor of 100-1000.

Alternatively, local linear models could be used in place of spline interpolation. Local linear models present the advantage that a modification of a single aircraft trajectory will affect the vector field only locally, in the area where the aircraft is flying, which allows a simpler update of complexity in trajectory management operations. In turn, the reconstructed vector field has no special smoothness properties, nor is the minimizer of any functional as in the case of splines.

It is important to note that for complexity prediction on mid term and long term time horizons, a time dependent vector field should be identified as pointed out in [18]. This is particularly critical to distinguish between a situation where two aircraft get close one to the other from a situation where the two aircraft occupy nearby positions but at different time instances within the reference look-ahead time horizon. Only in the former case, a conflict could take place.

The extension to the time-dependent case, however, is computationally even more challenging, which makes the approach not suitable for the time scale of the applications discussed in Chapter 2, at least at the current stage of development of the approach.

5 Novel methods for complexity evaluation

In this chapter we describe two novel methods for complexity evaluation that have been developed to better suit the requirements stemming from the airborne self separation application.

The key distinguishing feature is that the first method accounts for uncertainty in the prediction of the aircraft future position when evaluating complexity, whereas the second method neglects uncertainty and relies on the aircraft RBT to predict the aircraft position.

A detailed comparison between the two methods is postponed to Section 5.3, which includes the results of some test that was designed to assess the performance of the methods in terms of capability of identifying air traffic configurations that are difficult to control in a decentralized way.

5.1 A probabilistic approach to complexity evaluation

5.1.1 Introduction

In this section, we describe a method to air traffic complexity evaluation that was conceived within WP3. Its main distinguishing feature is that it explicitly accounts for the uncertainty affecting the future aircraft positions, [60]. Despite the extensive studies on uncertainty in the modeling and analysis of ATM systems by various researchers, see e.g. [21], [54], [56] and [44], its effect on air traffic complexity evaluation has not received adequate attention. Deterministic models for predicting the aircraft future positions along the look-ahead time horizon have been in fact adopted in the literature for complexity evaluation.

The introduced complexity measure is based on the notion of *probabilistic occupancy* of the airspace: complexity is evaluated in terms of proximity in time and space of the aircraft present in the traffic as determined by their intent and current state, while taking into account uncertainty in the aircraft future position. Indeed, since complexity evaluation on some look-ahead time horizon relies on trajectory prediction, the uncertainty in the aircraft position plays a critical role in complexity evaluation. Specifically, air traffic complexity at a point x in an airspace region $\mathcal{S} \subset \mathbb{R}^3$ and at time t within some look-ahead time horizon T is evaluated as the probability that a certain buffer zone in the airspace surrounding x will be "congested" within $[t, t+\Delta]$, with $\Delta > 0$. By defining congestion as the simultaneous occupancy of the buffer zone by a certain number of aircraft and evaluating this complexity measure at all possible points in $\mathcal{S}$, a complexity map can be built. Forming the complexity maps associated with different consecutive time intervals allows to predict when the aircraft will enter and leave a particular zone in the airspace, and to identify regions of the airspace $\mathcal{S}$ with a limited inter-aircraft maneuverability space. Avoiding these high complexity areas will prevent an additional aircraft entering $\mathcal{S}$ from excessive tactical maneuvering.

The attempt is to measure complexity as the effort required to determine a feasible, not necessarily optimal, resolution maneuver. This would make complexity evaluation independent of the adopted optimality criterion and of the actual controller in place, which is accounted for indirectly, through its effect on the air traffic organization.

5.1.2 Complexity from a global perspective

Consider N aircraft $A_i, i = 1, \ldots, N$, flying in the 3-D airspace $\mathcal{S} \subset \mathbb{R}^3$ during the look-ahead time horizon $T = [0, \bar{t}]$, with $t = 0$ representing the current time instant and $\bar{t} > 0$ the time horizon length. Suppose that each aircraft is following a nominal trajectory with a velocity profile $u^{A_i} : T \to \mathbb{R}^3$, starting from the initial position $x_0^{A_i}$ at time $t = 0$. The aircraft future position during T is not known exactly, and we assume that the prediction error can be modeled through a Gaussian random perturbation whose variance grows not only linearly with time t but also faster in the along-track direction (namely the direction of u^{A_i}) than in the cross-track directions (i.e., directions orthogonal to u^{A_i}). The predicted position $x^{A_i}(t) \in \mathbb{R}^3$ at time $t \in T$ of aircraft A_i is then given by

$$x^{A_i}(t) = x_0^{A_i} + \int_0^t u^{A_i}(s)ds + Q^{A_i}(t)\Sigma^{A_i}B^{A_i}(t), \quad t \geq 0, \tag{5}$$

where $B^{A_i}(t)$ is a standard 3-D Brownian motion starting from the origin whose variance is modulated by the matrix $Q^{A_i}(t)\Sigma^{A_i} \in \mathbb{R}^{3\times 3}$. More precisely, $\Sigma^{A_i} = \mathrm{diag}(\sigma_1^{A_i}, \sigma_2^{A_i}, \sigma_3^{A_i})$ is a diagonal matrix whose entries $\sigma_1^{A_i}$, $\sigma_2^{A_i}$, and $\sigma_3^{A_i}$ are the variance growth rates of the perturbation in the along-track direction and the two cross-track directions and satisfy $\sigma_1^{A_i} \geq \sigma_2^{A_i} = \sigma_3^{A_i} > 0$, whereas $Q^{A_i}(t) = \begin{bmatrix} q_1^{A_i}(t) & q_2^{A_i}(t) & q_3^{A_i}(t) \end{bmatrix} \in \mathbb{R}^{3\times 3}$ is an orthogonal matrix whose first column $q_1^{A_i}(t)$ is aligned with $u^{A_i}(t)$: $q_1^{A_i}(t) = \frac{u^{A_i}(t)}{\|u^{A_i}(t)\|}$. Similar models have been proposed in [22], [55] and [57] for predicting aircraft trajectories over a mid-term look-ahead time horizon of tens of minutes.

For each $x \in \mathcal{S}$, let us consider the ellipsoidal region $\mathcal{M}(x)$ centered at x and defined as:

$$\mathcal{M}(x) = \left\{\hat{x} \in \mathbb{R}^3 : \ (\hat{x} - x)^T M(\hat{x} - x) \leq 1\right\}, \tag{6}$$

where $M \in \mathbb{R}^{3\times 3}$ is a diagonal matrix given by

$$M = \mathrm{diag}\left(\frac{1}{{r_h}^2}, \frac{1}{{r_h}^2}, \frac{1}{{r_v}^2}\right),$$

with $r_h \geq r_v > 0$ defining the size of the ellipsoid in the horizontal plane and in the vertical direction. If $r_h = r_v$, then the ellipsoid reduces to a sphere of radius r_h, and proximity in the horizontal plane is weighted the same as that in the vertical direction. Typically, $r_h > r_v$ since vertical proximity between aircraft is considered in ATM to be less critical than horizontal proximity.

The complexity of air traffic within the airspace region $\mathcal{S}$ can be evaluated through the following occupancy measures.

Definition 1 (first order probabilistic occupancy measure) *The first order probabilistic occupancy $\gamma_1(x,t)$ at position $x \in \mathcal{S}$ within the time interval $[t, t+\Delta] \subseteq T$ is defined as*

$$\gamma_1(x,t) := P\left(x^{A_i}(t) \in \mathcal{M}(x),\ \textit{for some } t \in [t, t+\Delta] \textit{ and } i \in \{1,2,\ldots,N\}\right) \tag{7}$$

and represents the probability of at least one aircraft entering the ellipsoid $\mathcal{M}(x)$ within the time frame $[t, t+\Delta]$.

Note that $\gamma_1(x,t) = 0$ means that none of the existing aircraft will be inside the ellipsoid $\mathcal{M}(x)$ during the time interval $[t, t+\Delta]$. On the other hand, $\gamma_1(x,t) = 1$ implies that with certainty there will be at least one aircraft within $\mathcal{M}(x)$ at some time instant belonging to $[t, t+\Delta]$.

Similarly, we can define the second order probabilistic occupancy measure.

Definition 2 (second order probabilistic occupancy measure) *The second order probabilistic occupancy $\gamma_2(x,t)$ at position $x \in \mathcal{S}$ within the time interval $[t, t+\Delta] \subseteq T$ is defined as*

$$\begin{aligned}\gamma_2(x,t) :=& P\big(x^{A_i}(t) \textit{ and } x^{A_j}(t') \in \mathcal{M}(x) \textit{ for some } t,t' \in [t, t+\Delta] \textit{ and}\\ & i \neq j \in \{1,2,\ldots,N\}\big)\end{aligned} \tag{8}$$

and represents the probability of at least two aircraft entering the ellipsoid $\mathcal{M}(x)$ within the time frame $[t, t+\Delta]$.

If $\gamma_2(x,t) = 0$, then there will be at most a single aircraft inside the ellipsoid $\mathcal{M}(x)$ within the time interval $[t, t+\Delta]$. Hence, at any time $t \in [t, t+\Delta]$, an aircraft passing through $\mathcal{M}(x)$ will not be sharing $\mathcal{M}(x)$ with any of the other N aircraft. If $\gamma_2(x,t) = 1$, then with probability 1, at least two aircraft will enter the ellipsoid $\mathcal{M}(x)$ during the time interval $[t, t+\Delta]$, though possibly not at exactly the same time.

By letting x vary over $\mathcal{S}$, one can define the *first order and second order probabilistic occupancy maps* of the airspace region $\mathcal{S}$ within the time frame $[t, t+\Delta]$ as follows:

$$\begin{aligned}\Gamma_1(\cdot,t) &: x \in \mathcal{S} \to \gamma_1(x,t)\\ \Gamma_2(\cdot,t) &: x \in \mathcal{S} \to \gamma_2(x,t).\end{aligned}$$

Evidently, at any point $x \in \mathcal{S}$, the Γ_2 map has a value smaller than or equal to the Γ_1 map, since the corresponding events are nested.

Higher order probabilistic occupancy measures and maps can also be defined according to a similar procedure.

Forming the probabilistic occupancy maps for different consecutive time intervals allows to predict when the aircraft enter and leave a certain zone in the airspace, and to define the occupancy of the airspace region $\mathcal{S}$. This information can be used for detecting congested areas (i.e., areas where multi-aircraft encounters with limited inter-aircraft spacing are likely to occur) in the time-space coordinates, and to identify surrounding areas where the traffic could be deviated. The presence of a region with a high value of the second order probabilistic occupancy implies a high likelihood that two or more aircraft will get close in time and space, hence having a conflict. Trajectories should be designed so as to reduce second order probabilistic occupancy.

More compact global information can be obtained according to the following procedure. Let us parameterize the ellipsoidal region $\mathcal{M}(x)$ defined in (6) through a scaling factor $\rho > 0$ as follows:

$$\mathcal{M}_\rho(x) = \left\{\hat{x} \in \mathbb{R}^3 : \ (\hat{x} - x)^T M(\hat{x} - x) \leq \rho^2\right\}, \tag{9}$$

so that, by varying ρ, the ellipsoidal region can be either squeezed ($\rho < 1$) or enlarged ($\rho > 1$). Denote the complexity measures associated with region $\mathcal{M}_\rho$ and parameterized by ρ as $\gamma_1^\rho(x,t)$ and $\gamma_2^\rho(x,t)$. Both $\gamma_1^\rho(x,t)$ and $\gamma_2^\rho(x,t)$ are increasing as a function of ρ.

Let

$$\rho_{\max}(t) := \sup\{\rho \geq 0 : \sup_{x \in \mathcal{S}} \gamma_2^\rho(x,t) \leq p_T\},$$

where p_T is some threshold value for the probability that two aircraft come close one to the other, and define

$$\rho^\star_{\max} := \sup_{t \in T} \rho_{\max}(t).$$

Then, one can take

$$\xi := \frac{1}{\rho^\star_{\max}}$$

as a synthetic indicator of complexity of the traffic during the time horizon T. Note that the extent of the available maneuverability space as measured by ξ will depend on both the local aircraft density and the traffic dynamic through the aircraft intent. Since uncertainty in the predicted aircraft position models possible deviations of the aircraft from their intended trajectory, ξ can be interpreted as a measure of robustness of air traffic to perturbations of the nominal situation.

5.1.3 Complexity from a single aircraft perspective

Given the decentralized nature of airborne self separation, it also makes sense to introduce a complexity measure related to a single aircraft.

The global complexity measures in Section 5.1.2 can be easily adapted to provide a measure of complexity from the perspective of a single aircraft. To this end, suppose that an additional aircraft, say aircraft B, enters an airspace region $\mathcal{S}$ where N aircraft A_i, $i = 1, 2, \ldots, N$, are present. According to Definitions 1 and 2, complexity is evaluated from a global perspective as the probability of occupancy of a buffer zone surrounding a point by a certain number of aircraft (at least one aircraft for the first order complexity and at least two for the second order complexity). Suppose that aircraft B is following a nominal trajectory $\bar{x}^B : T \to \mathbb{R}^3$. The idea is to evaluate the complexity encountered by aircraft B along its nominal trajectory by making the buffer zone move along the trajectory of aircraft B and computing the probability that some of the other aircraft A_i, $i = 1, 2, \ldots, N$, will enter such moving zone. This leads to the following definition of single-aircraft complexity.

Definition 3 (single-aircraft probabilistic complexity measure) *The complexity experienced by aircraft B along its nominal trajectory $\bar{x}^B : T \to \mathcal{S}$ within the time interval $[t, t+\Delta]$ is defined as:*

$$\gamma_B(t) := P\left(x^{A_i}(t) \in \mathcal{M}(\bar{x}^B(t)) \text{ for some } t \in [t, t+\Delta] \text{ and } i \in \{1, 2, \ldots, N\}\right) \quad (10)$$

Interestingly, if the time window $[t, t+\Delta]$ extends to the whole look-ahead time horizon T and the buffer zone reproduces the protection zone surrounding each aircraft, the single-aircraft complexity measure can as well be interpreted as the probability of aircraft B getting in conflict with another aircraft A_i within T. CD&R then becomes an integrable task in complexity evaluation.

According to a reasoning similar to that in Section 5.1.2, based on the re-scaled ellipsoidal region (9) and the corresponding single-aircraft complexity function $\gamma_B^\rho : T \to [0, 1]$, we can introduce function $\rho_{\max,B} : T \to \mathbb{R}_+$ given by

$$\rho_{\max,B}(t) := \sup\{\rho \geq 0 : \gamma_B^\rho(t) \leq p_T\},$$

and define

$$\rho^\star_{\max,B} := \sup_{t \in T} \rho_{\max,B}(t).$$

$\rho^\star_{\max,B}$ is an index of robustness of the nominal trajectory of aircraft B. The larger is $\rho^\star_{\max,B}$, the more aircraft B is far from the other aircraft, both in time and in space, with high ($> 1 - p_T$) probability, and, hence, the larger is the robustness of its trajectory to possible deviations of the other aircraft from their intent.

The quantity

$$\xi_B := \frac{1}{\rho^\star_{\max,B}}$$

can then be taken as synthetic indicator of the air traffic complexity from the perspective of aircraft B during the time horizon T. Let ρ_{safe} denote the value of ρ such that $\mathcal{M}_\rho(x)$ represents the protection zone surrounding an aircraft positioned at x. If $\xi_B > \frac{1}{\rho_{\text{safe}}}$, then, some conflict can occur with probability $\geq p_T$ and the criticality of this conflict can be better assessed by computing, for instance, the earliest *conflict time*:

$$t^\star_B = \min\{t \geq 0 : \rho_{\max,B}(t) < \rho_{\text{safe}}\}.$$

The introduced single-aircraft complexity measure (10) can be used by aircraft B to evaluate the maneuverability space surrounding its nominal trajectory and to eventually redesign its trajectory so as to improve its robustness. According to a similar perspective, in the works on trajectory flexibility [35, 34] it is suggested that, to achieve the aggregate objective of avoiding excessive 'air traffic complexity' in autonomous aircraft ATM, aircraft should plan their trajectory so as to preserve maneuvering flexibility to accommodate possible disturbances stemming, for example, from other traffic.

5.1.4 Computational aspects

In this section we address the issue of determining analytic –though approximate– expressions of the probabilistic occupancy measures $\gamma_1(x,t)$ and $\gamma_2(x,t)$ representing the probability of multiple (at least one for γ_1 and at least two for γ_2) aircraft entering the same buffer zone $\mathcal{M}(x)$ within $[t, t+\Delta]$. Approaches for computing this probability are usually computationally intensive as the required computing time typically grows exponentially with the number of aircraft, e.g. [31]. Here, analytic formulas approximating this probability will be derived, which results in a linear growth of computation time with the number of aircraft. These formulas can be extended to estimate the single-aircraft complexity measure $\gamma_B(t)$, as explained at the end of this section.

Denote as $P^{A_i}(x, [t_s, t_f])$ the probability that aircraft A_i enters the ellipsoid $\mathcal{M}(x)$ centered at $x \in \mathcal{S}$ within the time frame $[t_s, t_f]$:

$$P^{A_i}(x, [t_s, t_f]) := P\left(x^{A_i}(t) \in \mathcal{M}(x) \text{ for some } t \in [t_s, t_f]\right). \tag{11}$$

If the Brownian motions affecting the future positions of the N aircraft are assumed to be independent, then the first order and second order probabilistic occupancy measures (7) and (8) satisfy:

$$\gamma_1(x,t) = 1 - \prod_{i=1}^{N} (1 - P^{A_i}(x, [t, t+\Delta])) \tag{12}$$

$$\begin{aligned}\gamma_2(x,t) = 1 &- \prod_{i=1}^{N} (1 - P^{A_i}(x, [t, t+\Delta])) \\ &- \sum_{i=1}^{N} P^{A_i}(x, [t, t+\Delta]) \prod_{j=1, j\neq i}^{N} (1 - P^{A_j}(x, [t, t+\Delta])),\end{aligned} \tag{13}$$

and the problem of evaluating complexity reduces to that of estimating the probability $P^{A_i}(x, [t_s, t_f])$.

Remark 1 *Note that the assumption of independent Brownian motions is reasonable if the correlation due to the effect of wind is negligible and, in particular, if the N aircraft are flying far apart, [31], [11]. In presence of non-negligible wind correlation, the above expressions represent only approximations of the probabilistic occupancy measures γ_1 and γ_2.*

We next determine an analytic approximation of the probability $P^{A_i}(x,[t_s,t_f])$ in (11). The obtained approximate expression is then used to estimate $\gamma_1(x,t)$ and $\gamma_2(x,t)$ through (12) and (13). Derivations refer first to the case of aircraft following straight line nominal trajectories with constant velocity and are then extended to multi-legged nominal trajectories specified by a sequence of timed way points.

Analytical approximation of $P^{A_i}(x,[t_s,t_f])$ For ease of notation, in this subsection we shall refer to aircraft A_i as aircraft A, dropping the subscript.

One-leg nominal trajectory case: Under the assumption that aircraft A is following a straight line nominal trajectory with constant velocity, equation (5) can be rewritten as

$$x^A(t) = x_0^A + u^A t + Q^A \Sigma^A B^A(t), \quad t \geq 0.$$

From this equation, we have that the relative position $\Delta x(t) = x - x^A(t)$ of aircraft A with respect to the point x is given by

$$\Delta x(t) = \Delta x_0 + \Delta u\, t - n(t), \tag{14}$$

where we set $\Delta x_0 = x - x_0^A$, $\Delta u = -u^A$ and $n(t) = Q^A \Sigma^A B(t)$.
Equation (14) suggests that we can evaluate $P^A(x,[t_s,t_f])$ by determining the probability that the perturbation $n(t)$ hits an ellipsoid whose center is moving at a constant velocity Δu starting from Δx_0: $n(t) \in \mathcal{M}(\Delta x_0 + \Delta u\, t)$, for some $t \in [t_s,t_f]$.
Define the vector

$$v = \Omega^{-1} \Delta u$$

with $\Omega := Q^A \Sigma^A$. An orthogonal matrix $P = \begin{bmatrix} p_1 & p_2 & p_3 \end{bmatrix} \in \mathbb{R}^{3\times 3}$ can be constructed whose first column $p_1 = -v/\|v\|$ is aligned with $-v$ (the choice of p_2 and p_3, hence P, is not unique). Its inverse $P^{-1} = P^T$ represents a rotation that makes the $-v/\|v\|$ direction coincide with the first coordinate axis direction:

$$P^{-1} \frac{-v}{\|v\|} = e_1 := \begin{bmatrix} 1 & 0 & 0 \end{bmatrix}^T.$$

Using the coordinate transformation $\Delta z(t) = P^{-1}\Omega^{-1}\Delta x(t)$, we transform (14) to the following:

$$\Delta z(t) = a + wt - \hat{B}(t), \tag{15}$$

where $\hat{B}(t) := P^{-1}B(t)$ is still a standard Brownian motion starting from the origin (rotation of a Brownian motion is still a Brownian motion), and $a \in \mathbb{R}^3, w \in \mathbb{R}^3$ are defined by

$$a = P^{-1}\Omega^{-1}\Delta x_0, \qquad w = P^{-1}\Omega^{-1}\Delta u = P^{-1}v = -\|v\|e_1.$$

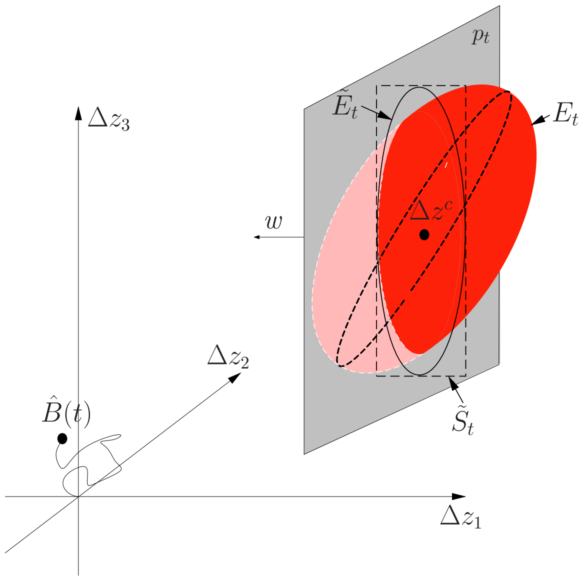

Figure 5: Ellipsoidal protection zone E_t in the new coordinates.

From equation (15), we can again think of computing $P^A(x, [t_s, t_f])$ as determining the probability that the standard Brownian motion $\hat{B}(t)$ starting from the origin hits a moving ellipsoid E_t obtained by transforming $\mathcal{M}(\Delta x_0 + \Delta u t)$ in the new coordinate system, that is:

$$P^A(x, [t_s, t_f]) = P\left(\hat{B}(t) \in E_t \text{ for some } t \in [t_s, t_f]\right), \tag{16}$$

where

$$E_t = \left\{ z : \ (z - (a + wt))^T \, P^T \Omega^T M \Omega P \, (z - (a + wt)) \leq 1 \right\}.$$

The center of E_t is moving at the constant velocity w starting from a. From our choice of matrix P, the velocity w is directed along the negative Δz_1 axis (see Figure 5).

We next find an analytical approximation for the probability in (16). For a fixed time $t \in [t_s, t_f]$, define p_t as the plane that passes through the center $\Delta z^c = a + wt$ of the ellipsoid E_t and is orthogonal to its velocity w (hence orthogonal to the Δz_1-axis). Then p_t divides the ellipsoid E_t into two equal parts. We shall first find the projection of E_t onto the plane p_t and then the minimum bounding rectangle containing such a projection.

Let $\pi_t : \mathbb{R}^3 \to p_t$ be the orthogonal projection operator onto the two dimensional plane p_t which can be identified with $\mathbb{R}^2$. Then, the projection $\tilde{E}_t := \pi_t(E_t)$ of E_t onto p_t is itself an ellipse centered at $\tilde{z}^c := \pi_t(\Delta z^c) \in \mathbb{R}^2$. Specifically, a point $\tilde{z} \in \mathbb{R}^2$ belongs to $\tilde{E}_t$ if and only if there exists some $z_1 \in \mathbb{R}$ such that $\Delta z = \begin{bmatrix} z_1 \\ \tilde{z} \end{bmatrix} \in E_t$ or, equivalently,

$$(\Delta z - \Delta z^c)^T \, P^T \Omega^T M \Omega P \, (\Delta z - \Delta z^c) \leq 1. \tag{17}$$

Write $P^T\Omega^T M\Omega P$ in block matrix form as:

$$P^T\Omega^T M\Omega P = \begin{bmatrix} \alpha & y^T \\ y & R \end{bmatrix},$$

where $R \in \mathbb{R}^{2\times 2}$, $y \in \mathbb{R}^2$, and $\alpha \in \mathbb{R}$. Since $P^T\Omega^T M\Omega P$ is positive definite, we must have that R is positive definite and $\alpha > 0$. Then condition (17) is equivalent to

$$\alpha(z_1 - \Delta z_1^c)^2 + 2y^T(\tilde{z} - \tilde{z}^c)(z_1 - \Delta z_1^c) + (\tilde{z} - \tilde{z}^c)^T R(\tilde{z} - \tilde{z}^c) \leq 1, \tag{18}$$

for some $z_1 \in \mathbb{R}$. The left-hand-side of (18) is a quadratic function in z_1 whose minimum with respect to z_1 is given by

$$(\tilde{z} - \tilde{z}^c)^T R(\tilde{z} - \tilde{z}^c) - \frac{1}{\alpha}\left[y^T(\tilde{z} - \tilde{z}^c)\right]^2 = (\tilde{z} - \tilde{z}^c)^T \tilde{R}(\tilde{z} - \tilde{z}^c),$$

where $\tilde{R} \in \mathbb{R}^{2\times 2}$ is the positive definite matrix defined by

$$\tilde{R} := R - \frac{yy^T}{\alpha}.$$

Condition (18) is equivalent to that its left-hand-side minimum with respect to z_1 is smaller that its right-hand-side. This yields the exact expression of the projection ellipse $\tilde{E}_t$ as:

$$\tilde{E}_t = \left\{\tilde{z} \in \mathbb{R}^2 \;:\; (\tilde{z} - \tilde{z}^c)^T \tilde{R}(\tilde{z} - \tilde{z}^c) \leq 1\right\}.$$

We now determine the rectangle on p_t that encloses $\tilde{E}_t$ and has the smallest area, namely, the *minimum bounding rectangle* of $\tilde{E}_t$. This rectangle, denoted by $\tilde{S}_t$, will be used in the approximation of the probability $P^A(x, [t_s, t_f])$.
We decompose the positive definite matrix $\tilde{R}$ as

$$\tilde{R} = \begin{bmatrix} v_1 & v_2 \end{bmatrix} \operatorname{diag}(\lambda_1, \lambda_2) \begin{bmatrix} v_1 & v_2 \end{bmatrix}^T, \tag{19}$$

where λ_1 and λ_2 are the eigenvalues of $\tilde{R}$ with $\lambda_1 \geq \lambda_2 > 0$, and v_1 and v_2 are the corresponding eigenvectors which can be assumed to be an orthonormal pair. Then v_2 identifies the direction of the major axis of the ellipse $\tilde{E}_t$, along which $\tilde{E}_t$ has length $\frac{2}{\sqrt{\lambda_2}}$, whereas v_1 identifies the minor axis direction, along which $\tilde{E}_t$ has length $\frac{2}{\sqrt{\lambda_1}}$. As a result, the minimum bounding rectangle $\tilde{S}_t$ of the ellipse $\tilde{E}_t$ is the one centered at $\tilde{z}^c$, with length $\frac{2}{\sqrt{\lambda_2}}$ along the v_2 direction and $\frac{2}{\sqrt{\lambda_1}}$ along the v_1 direction.
Recall that the probability of interest $P^A(x, [t_s, t_f])$ that aircraft A enters the ellipsoid $\mathcal{M}(x)$ within $[t_s, t_f]$ is expressed in (16) as the probability that the Brownian motion $\hat{B}(t)$ starting from the origin hits the ellipsoid E_t whose center moves in the negative Δz_1-axis direction starting from a at time 0. The analytical expression of such a probability is difficult to obtain. We then suggest to approximate it by the probability that, when $\hat{B}(t)$ first hits the moving plane p_t, the hitting location is inside the minimum bounding rectangle $\tilde{S}_t$ of the projected ellipse $\tilde{E}_t$.

Remark 2 *The idea underlying this approximation scheme is that, since the velocity w of the ellipsoid is typically much larger than the growth rate of the variance of the Brownian motion, then, the only dimension of the ellipsoid that is relevant for the event of interest is that perpendicular to w. Using the minimum bounding rectangle $\tilde{S}_t$ in place of the projected ellipse $\tilde{E}_t$ then introduces an over-approximation error.*
A similar approximation scheme was used in [57] with reference to the problem of computing the probability of conflict in the 2-D case. A formal discussion on the quality of the approximation is reported in [30].

Define $\tau := \inf\{t \geq 0 \,:\, \hat{B}(t) \in p_t\}$ to be the first time that the Brownian motion $\hat{B}(t)$ ever hits the moving plane p_t. Since the three coordinates of $\hat{B}(t)$ are independent one-dimensional Brownian motions, and the directions orthogonal to plane p_t and along which the plane p_t is moving are both aligned with the Δz_1-axis, it is easy to see that τ depends only on the first component $\hat{B}_1(t)$ of $\hat{B}(t)$. Specifically, τ is the first time that the one-dimensional Brownian motion $\hat{B}_1(t)$ starting from the origin hits a point $z_1(t) \in \mathbb{R}$ that moves according to the dynamics $z_1(t) = a_1 - \|v\|t$, where a_1 is the first component of $a \in \mathbb{R}^3$.

Note that $a_1 < 0$ implies that the aircraft A is moving away from the ellipsoid $\mathcal{M}(x)$ in the x-coordinates and results in approximately zero probability of entering $\mathcal{M}(x)$. For the purpose of complexity evaluation, we then set $P^A(x, [t_s, t_f]) = 0$ when $a_1 < 0$.

When $a_1 \geq 0$, the probability distribution of τ is characterized by the following lemma.

Lemma 2 (Bachelier-Levy, [20]) *Define $\tau := \inf\{t \geq 0 :\ \hat{B}_1(t) = a_1 - \|v\|t\}$ to be the first time the 1-D Brownian motion $\hat{B}_1(t)$ starting from the origin reaches a point moving at the speed $\|v\|$ towards the origin starting from some $a_1 \geq 0$. Then, τ has the probability density function:*

$$p_\tau(t) = \frac{a_1}{\sqrt{2\pi t^3}} e^{-\frac{(a_1 - \|v\|t)^2}{2t}}, \quad t \geq 0. \tag{20}$$

Lemma 3 ([30]) *Let $p_\tau(t)$ be the probability density function of τ as given in (20) and assume $a_1 \geq 0$. Then for any $t_f \geq 0$,*

$$\begin{aligned}
\int_0^{t_f} p_\tau(t)\,dt &= Q\left(a_1 t_f^{-1/2} - \|v\| t_f^{1/2}\right) + e^{2a_1\|v\|} Q\left(a_1 t_f^{-1/2} + \|v\| t_f^{1/2}\right), \qquad (21)\\
\int_0^{t_f} t\,p_\tau(t)\,dt &= \frac{a_1}{\|v\|} Q\left(a_1 t_f^{-1/2} - \|v\| t_f^{1/2}\right) - \frac{a_1}{\|v\|} e^{2a_1\|v\|} Q\left(a_1 t_f^{-1/2} + \|v\| t_f^{1/2}\right),
\end{aligned}$$

where $Q(x) := \int_x^\infty \frac{1}{\sqrt{2\pi}} e^{-\frac{x^2}{2}}\,dx$ is the Q-function, which is related to the error function erf$(\cdot)$ by: $Q(x) = \frac{1}{2} - \frac{1}{2}\mathrm{erf}(\frac{x}{\sqrt{2}})$. In particular, letting $t_f \to \infty$, we have $\int_0^\infty p_\tau(t)\,dt = 1$ and

$$E[\tau] = \int_0^\infty t\,p_{t^\star}(t)\,dt = \frac{a_1}{\|v\|}.$$

Let $\pi_\tau(\hat{B}(t)) \in \mathbb{R}^2$ be the projection of the Brownian motion $\hat{B}(t)$ at the hitting time τ onto the plane p_t. Conditioning on $\tau = t$, the distribution of $\pi_\tau(\hat{B}(t))$ is a two-dimensional Gaussian random variable with zero mean and covariance tI_2; hence $\pi_\tau(\hat{B}(t)) \sim W_1 v_1 + W_2 v_2$, where v_1 and v_2 are the orthonormal pair given in (19), and $W_1, W_2 \sim N(0,t)$ are independent one-dimensional Gaussian random variables. Moreover, by our previous discussions, the minimum bounding rectangle $\tilde{S}_t$ can be expressed as the set of all $\alpha_1 v_1 + \alpha_2 v_2$ with $|\alpha_1 - v_1^T \tilde{a}| \leq \frac{1}{\sqrt{\lambda_1}}$ and $|\alpha_2 - v_2^T \tilde{a}| \leq \frac{1}{\sqrt{\lambda_2}}$ where $\tilde{a} = \pi(a)$ is the projection of a onto p_t, which coincides with $\tilde{z}^c$.
As a result, $g(t) := P\left(\pi_\tau(\hat{B}(t)) \in \tilde{S}_\tau \,\middle|\, \tau = t\right)$ can be computed as follows

$$\begin{aligned} g(t) &= P\left(W_1 v_1 + W_2 v_2 \in \tilde{S}_t\right) \\ &= P\left(\left|W_1 - v_1^T \tilde{a}\right| \leq \frac{1}{\sqrt{\lambda_1}}\right) \cdot P\left(\left|W_2 - v_2^T \tilde{a}\right| \leq \frac{1}{\sqrt{\lambda_2}}\right) \\ &= \left[Q\left(\frac{v_1^T \tilde{a}\sqrt{\lambda_1} - 1}{\sqrt{\lambda_1 t}}\right) - Q\left(\frac{v_1^T \tilde{a}\sqrt{\lambda_1} + 1}{\sqrt{\lambda_1 t}}\right)\right]\left[Q\left(\frac{v_2^T \tilde{a}\sqrt{\lambda_2} - 1}{\sqrt{\lambda_2 t}}\right) - Q\left(\frac{v_2^T \tilde{a}\sqrt{\lambda_2} + 1}{\sqrt{\lambda_2 t}}\right)\right]. \end{aligned} \tag{22}$$

Finally, an approximated expression for $P^A(x, [t_s, t_f])$ can be computed as

$$\hat{P}^A(x, [t_s, t_f]) = \int_{t_s}^{t_f} g(t) p_\tau(t)\, dt. \tag{23}$$

Evaluating expression (23) involves an integration, which may be time-consuming. Thus, simplified expressions that are easier to compute are needed. One way to approximate (23) is to expand $g(t)$ around $t_e := E[\tau | t_s \leq \tau \leq t_f]$. If a zero-th order expansion is used, then

$$\hat{P}^A(x, [t_s, t_f]) \simeq g(t_e) \int_{t_s}^{t_f} p_\tau(t)\, dt, \tag{24}$$

which can then be evaluated using (21) in Lemma 3. The time instant t_e is the expected time that the Brownian motion $\hat{B}(t)$ hits the plane p_t conditioning on that it hits within the time interval $[t_s, t_f]$ and is given by

$$t_e = \frac{\int_{t_s}^{t_f} t\, p_\tau(t)\, dt}{\int_{t_s}^{t_f} p_\tau(t)\, dt},$$

where $\int_{t_s}^{t_f} t\, p_\tau(t)\, dt = \int_0^{t_f} t\, p_\tau(t)\, dt - \int_0^{t_s} t\, p_\tau(t)\, dt$ can be evaluated using Lemma 3.
Using a first order approximation of $g(t) \simeq g(t_e) + (t - t_e)\dot{g}(t_e)$ around $t = t_e$, we obtain

$$\hat{P}^A(x, [t_s, t_f]) \simeq [g(t_e) - t_e \dot{g}(t_e)] \int_{t_s}^{t_f} p_\tau(t)\, dt + \dot{g}(t_e) \int_{t_s}^{t_f} t\, p_\tau(t)\, dt, \tag{25}$$

where $\dot{g}(t) = \frac{dg(t)}{dt}$ can be computed from (22) using the fact that $Q(x) = \int_x^\infty e^{-z^2/2} dz$ as

$$\dot{g}(t_e) = -\frac{\sqrt{2\pi}}{2t_e}\left\{[Q(u_1) - Q(u_2)](u_4 e^{-u_4{}^2} - u_3 e^{-u_3{}^2}) + [Q(u_3) - Q(u_4)](u_2 e^{-u_2{}^2} - u_1 e^{-u_1{}^2})\right\},$$

with

$$u_1 := \frac{v_1^T \tilde{a}\sqrt{\lambda_1} - 1}{\sqrt{\lambda_1} t},\ u_2 := \frac{v_1^T \tilde{a}\sqrt{\lambda_1} + 1}{\sqrt{\lambda_1} t},\ u_3 := \frac{v_2^T \tilde{a}\sqrt{\lambda_2} - 1}{\sqrt{\lambda_2} t} \text{ and } u_4 := \frac{v_2^T \tilde{a}\sqrt{\lambda_2} + 1}{\sqrt{\lambda_2} t}.$$

Multi-legged nominal trajectory case: We consider now the case when the nominal velocity of aircraft A is not constant throughout the whole time horizon T but only during each element $[t_j, t_{j+1}]$, $j = 1, 2, \dots, m$, of a finite partition of T.

Suppose that $[t_s, t_f] \subseteq [t_j, t_{j+1}]$ for some $j \in \{1, 2, \dots, m\}$, and denote by u_j^A the constant nominal velocity of A within $[t_j, t_{j+1}]$. Then, the predicted position of aircraft A along the time interval $[t_s, t_f]$ can be expressed as

$$x^A(t) = \tilde{x}_0^A + u_j^A t + Q^A \Sigma^A B^A(t), \tag{26}$$

where

$$\tilde{x}_0^A = x_0^A + \int_0^{t_s} u^A(s) ds - u_j^A t_s$$

is a fictitious initial condition such that the straight line trajectory travelled from $\tilde{x}_0^A$ at constant velocity u_j^A coincides with the actual nominal trajectory of aircraft A within the time interval $[t_s, t_f]$. Then, the procedure described in the one-leg case can be applied to determine an estimate of $P^A(x, [t_s, t_f])$ based on (26).

If the condition $[t_s, t_f] \subseteq [t_j, t_{j+1})$ is not satisfied, we can partition $[t_s, t_f]$ in subintervals $[\tau_h, \tau_{h+1}]$, $h = 1, \dots, p$, each one corresponding to a leg of the nominal trajectory and over-approximate as follows:

$$\hat{P}^A(x, [t_s, t_f]) = \sum_{h=1}^{p} P^A(x, [\tau_h, \tau_{h+1}]).$$

Each $P^A(x, [\tau_h, \tau_{h+1}])$ can then be estimated through the procedure described above.

Analytic approximation of the probabilistic occupancy measures An analytic approximation of $\gamma_1(x, t)$ and $\gamma_2(x, t)$ can be easily obtained by plugging the estimates $\hat{P}^{A_i}(x, [t_s, t_f])$ of $P^{A_i}(x, [t_s, t_f])$, $i = 1, 2, \dots, N$, into the formulas (12) and (13), thus getting

$$\hat{\gamma}_1(x, t) = 1 - \prod_{i=1}^{N} (1 - \hat{P}^{A_i}(x, [t, t + \Delta])) \tag{27}$$

$$\begin{aligned} \hat{\gamma}_2(x, t) = {} & 1 - \prod_{i=1}^{N} (1 - \hat{P}^{A_i}(x, [t, t + \Delta])) \\ & - \sum_{i=1}^{N} \hat{P}^{A_i}(x, [t, t + \Delta]) \prod_{j=1, j \neq i}^{N} (1 - \hat{P}^{A_j}(x, [t, t + \Delta])), \end{aligned} \tag{28}$$

These expressions show that the computational effort involved in the evaluation of complexity at position $x \in \mathcal{S}$ scales linearly with the number of aircraft N and, hence, it does not radically increases when an additional aircraft is introduced. Suppose in fact that computing $\hat{P}^{A_i}(x,[t_s,t_f])$ for aircraft A_i takes a unit time. In an airspace region with N aircraft, a total of N time units is taken to compute $\hat{P}^{A_i}(x,[t_s,t_f])$ for all the N aircraft. Once all $\hat{P}^{A_i}(x,[t_s,t_f])$, $i = 1, 2, \ldots, N$, are obtained, both the $\gamma_1(x,t)$ and the $\gamma_2(x,t)$ metrics can be computed with a constant number of additional operations. Higher order complexity measures could be also estimated based on $\hat{P}^{A_i}(x,[t_s,t_f])$, $i = 1, 2, \ldots, N$, at no additional cost.

This is an important property, since real time computability is typically required in time-critical operations such as CD&R.

Computing the single-aircraft complexity measure The procedure for approximating the first order probabilistic occupancy $\gamma_1(x,t)$ can be easily adapted to compute an analytical approximation of the single-aircraft probabilistic complexity $\gamma_B(t)$ defined in (10). Indeed, $\gamma_B(t)$ can be expressed as

$$\gamma_B(t) = 1 - \prod_{i=1}^{N} (1 - P^{A_i}(\bar{x}^B(t), [t, t+\Delta])),$$

and to compute $P^{A_i}(\bar{x}^B(t), [t, t+\Delta])$ one just needs to consider the relative position of aircraft A_i with respect to aircraft B rather than with respect to the fix position x. If aircraft B enters $\mathcal{S}$ at time 0 starting from x with a constant velocity u^B, then, this will lead to an equation of the same form of equation (14) with the only difference being that $\Delta u = u^B - u_i^A$.

Construction of the probabilistic occupancy maps and of the scalar-valued function describing the complexity experienced by a single aircraft In order to build the probabilistic occupancy maps, one has to evaluate $\gamma_1(x,t)$ and $\gamma_2(x,t)$ across $\mathcal{S}$, at Δ-spaced sampled times along the reference time horizon T. This calls for some discretization of $\mathcal{S}$. Using an uniform gridding of step size $\delta > 0$ along all axes will result in $\mathbf{O}(\delta^{-3})$ grid points. Halving the step size, for example, would then result in eight times more grid points. It then follows that evaluating the complexity maps $\Gamma_1(\cdot,t)$ and $\Gamma_2(\cdot,t)$ in an airspace region $\mathcal{S}$ with N aircraft would require a computational time proportional to $N\delta^{-3}$.

One possible way to alleviate the exponential growth of computation time as the grid size decreases would be to use a variable sized grid. A coarser grid could be used to evaluate the complexity in regions that do not require a significant accuracy (e.g. regions sufficiently far from the nominal trajectories of the aircraft), while a finer grid could be used in regions requiring higher accuracy. The identification of such regions might be done using the complexity maps from the previous time interval.

As for the scalar-valued function describing the complexity experienced by a single aircraft along its planned trajectory, perspective, one has to evaluate $\gamma_B(t)$ at Δ-spaced sampled times along the reference time horizon T, hence is not affected by the exponential growth of sampled points as in the case of spatial gridding.

5.1.5 Numerical examples

A 2D numerical example Consider a rectangular airspace region $\mathcal{S}$ where 6 aircraft are following a one-leg nominal trajectory from some starting to some destination position during the look-ahead time horizon $T = [0, \bar{t}]$ with $\bar{t} = 15$ minutes (min), while trying to keep at a minimum safe distance $\rho_{\text{safe}} = 3$ nautical miles (nmi). The configuration of the aircraft nominal trajectories is shown in Figure 6, where starting positions are marked with $*$ and destination positions with $\diamond$.

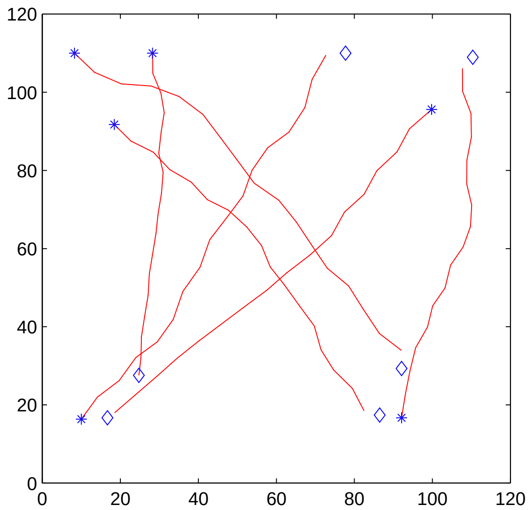

Figure 6: Sample paths of 6 aircraft moving from starting position ($*$) to destination position ($\diamond$), while trying to keep at a distance 3 nmi.

The trajectories in this figure are obtained by implementing the decentralized resolution strategy introduced in [57], which accounts for the uncertainty affecting the aircraft motion according to a similar model for the aircraft predicted motion. According to this strategy, resolution maneuvers involve only heading changes.

In the 2D level-flight case, the ellipsoidal region $\mathcal{M}(x)$ in (6) for complexity computation becomes a circle of radius r_x. In this example we set $r_x = 1$ so that the scaling factor ρ becomes the actual radius of the re-scaled ellipsoidal region $\mathcal{M}_\rho(x)$ in (9).

The global complexity of the considered air traffic system obtained with $p_T = 0.2$ is $\xi_2 \simeq 3$, which means that aircraft are only guaranteed to keep at a distance of about 0.33 nmi, with probability greater than 0.8.

The probabilistic occupancy map $\Xi_2 : \mathcal{S} \to [0, 1]$ plotted in Figure 7 is obtained by condensing the timing information as follows:

$$\Xi_2(x) = \frac{1}{\bar{t}} \int_0^{\bar{t}} \gamma_2(x,t)dt. \tag{29}$$

with the radius of the region $\mathcal{M}(x)$ set equal to 3 nmi.

This map reveals that there are two main regions with some significant percentage of occupancy (larger than 10%): one in the upper left-hand-side, and the other close to the center of the airspace area $\mathcal{S}$.

$\Xi_2(x) = 0$ means that there will be at most a single aircraft within the ball of radius 3 nmi centered at x during the whole interval $[0, \bar{t}]$. Aircraft passing through x such that $\Xi_2(x) > 0$ will be possibly involved in a conflict and the likelihood of this event grows with $\Xi_2(x)$. If $\Xi_2(x) = 1$, in particular, there will be more than 2 aircraft within the ball of radius 3 nmi centered at x during the whole interval $[0, \bar{t}]$.

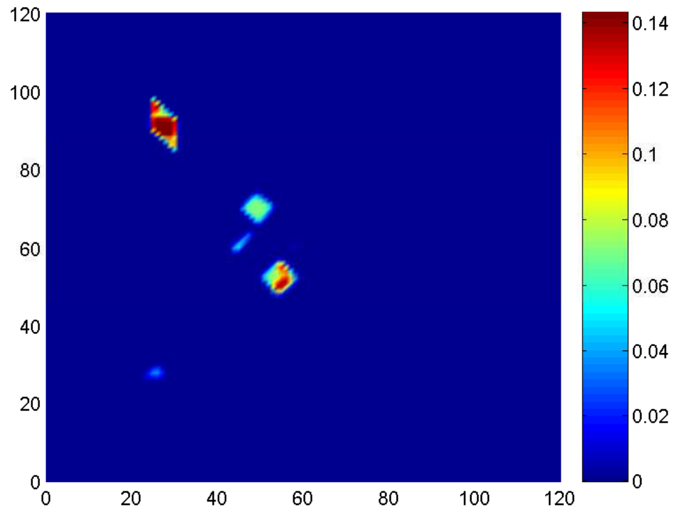

Figure 7: Complexity map $\Xi_2 : \mathcal{S} \to [0,1]$ obtained for $\rho_{\text{safe}} = 3$ nmi.

The earliest conflict time for both the two aircraft in the upper left-hand-side of the airspace area $\mathcal{S}$ is $t_B^\star = 2$ min. Indeed, the snapshot of the resolution maneuvers taken at time $t = 2$ min shows that this is the earliest time that a significant deviation action is taken by the decentralized solver and that it involves the two aircraft in the upper left-hand-side (Figure 8).

In this example, the complexity map Ξ_2 has been evaluated at uniformly sampled grid points $x \in \mathcal{S} = [0, 120] \times [0, 120]$ with a grid size $\delta_{x_1} = \delta_{x_2} = 1$. In the numerical evaluation of the integral over $[0, \bar{t}]$ involved in (29), $[0, \bar{t}]$ has been uniformly sampled with $\delta_t = 1$. The short term look-ahead time horizon Δ has been set equal to 2 min, and the spectral densities $\sigma_1^{A_i} = 0.25$ nmi $\cdot$ (min)$^{-1/2}$ in the along track direction, and $\sigma_2^{A_i} = 0.2$ nmi $\cdot$ (min)$^{-1/2}$ in the cross track directions.

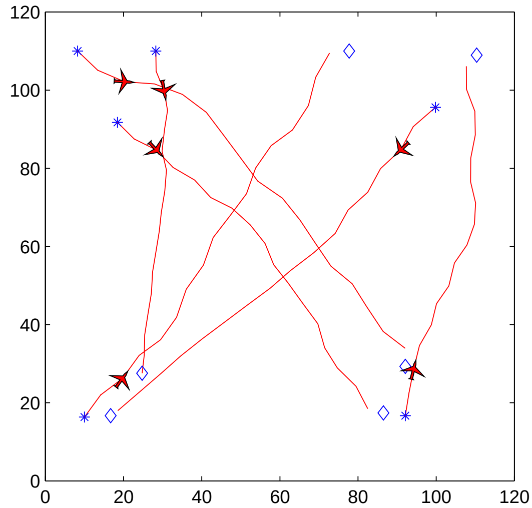

Figure 8: Snapshot of the resolution maneuvers for the 6 aircraft system in Figure 6 at time $t = 2$ min.

3D numerical examples In all the examples to follow, the parameters r_h and r_v defining the ellipsoidal buffer region $\mathcal{M}(x)$ in (6) are set equal to $r_h = 5$ nmi and $r_v = 2000$ feet (0.3291 nmi), and the look-ahead time horizon is $T = [0, 10]$ min. The zero-th order approximation formula (24) is used when computing the complexity measures by (27) and (28).

Evaluating the airspace occupancy:

Consider a 3-D airspace region with six aircraft. Each aircraft is moving at constant velocity along a straight line during the time interval T. The nominal trajectories of the aircraft are shown in Figure 9. Figure 10(a) shows the first order probabilistic occupancy map $\Gamma_1(\cdot, t)$ for five different consecutive time frames $[t, t + \Delta]$ of length $\Delta = 2$ min, covering the whole time horizon T. The uncertainty affecting the aircraft future positions is characterized through the spectral densities $\sigma_1^{A_i} = 0.5$ nmi$\cdot$(min)$^{-1/2}$ in the along track direction, and $\sigma_2^{A_i} = \sigma_3^{A_i} = 0.2$ nmi $\cdot$ (min)$^{-1/2}$ in the cross track directions. For each time frame, the complexity map is evaluated at uniformly sampled points in the horizontal plane XY with an uniform gridding of size $\delta_x = \delta_y = 0.2$ nmi. Similarly, the probabilistic occupancy maps $\Gamma_2(\cdot, t)$, $t = 0, 2, 4, 6, 8$, are plotted in Figure 10(b).

Figure 10(a) shows that the first order probabilistic occupancy is high initially in those zones that the aircraft are most likely to occupy in the XY plane. However, it can be seen from the second order probabilistic occupancy map that no two aircraft come close to each other in the first two time frames. During the time frame $[4, 6]$, there is a zone of high Γ_1 and Γ_2 complexity in the airspace. From the Γ_2 map, we can deduce that there will be more than one aircraft during this interval in that zone. This is to be

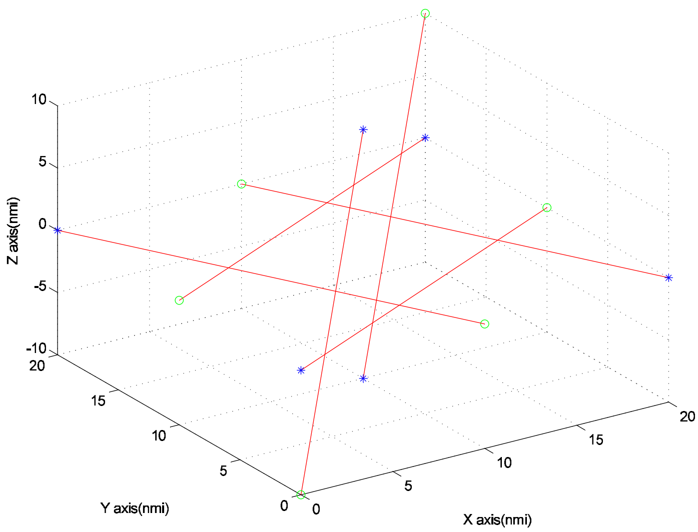

Figure 9: Initial positions and nominal trajectories of the aircraft. '*' denote starting points, and 'o' denote the nominal position of the aircraft at time t= 10 min.

expected considering that the nominal trajectories take the aircraft close to each other around this time. Also, the drastic decrease in the Γ_1 complexity map in successive subintervals indicates that the aircraft then move away from each other. Additional traffic entering the airspace should then better avoid crossing the XY plane in the time frame $[2, 4]$.

Evaluation of the maneuverability space: Suppose that an additional aircraft B is introduced at time $t = 0$ at the point $[8, 8, -2]^T$ nmi in the airspace where the six aircraft are flying. Aircraft B is following a straight line trajectory at the constant velocity $u^B = [2, 2, 2]^T$ nmi/min. Due to the presence of the six aircraft, aircraft B is not free to change its heading arbitrarily during the flight. In Figure 11 we represent the complexity $\gamma_B(t)$ defined in (10) as a function of the heading of aircraft B over a time frame of length $\Delta = 1$ minute at a few sampled-points along the nominal trajectory of aircraft B, when $\sigma_1^{A_i} = 0.5$ nmi $\cdot$ (min)$^{-1/2}$ and $\sigma_2^{A_i} = \sigma_3^{A_i} = 0.2$ nmi $\cdot$ (min)$^{-1/2}$. It can be observed that aircraft B faces a decrease in the amount of low-complexity prospective headings at some of these points, indicating that the airspace surrounding them is congested. This information might be used by aircraft B to find a minimal-complexity trajectory through the airspace.

If the spectral density increases to $\sigma_1^{A_i} = 1$ nmi $\cdot$ (min)$^{-1/2}$ and $\sigma_2^{A_i} = \sigma_3^{A_i} = 0.4$ nmi $\cdot$ (min)$^{-1/2}$, then, the maneuverability space reduces due to the wider spread of uncertainty in the future aircraft position. This can be seen by comparing Figure 12 with the plot in the second row, left side, of Figure 11. By tuning the spectral density parameters, one can then affect the level of flexibility of the designed trajectory.

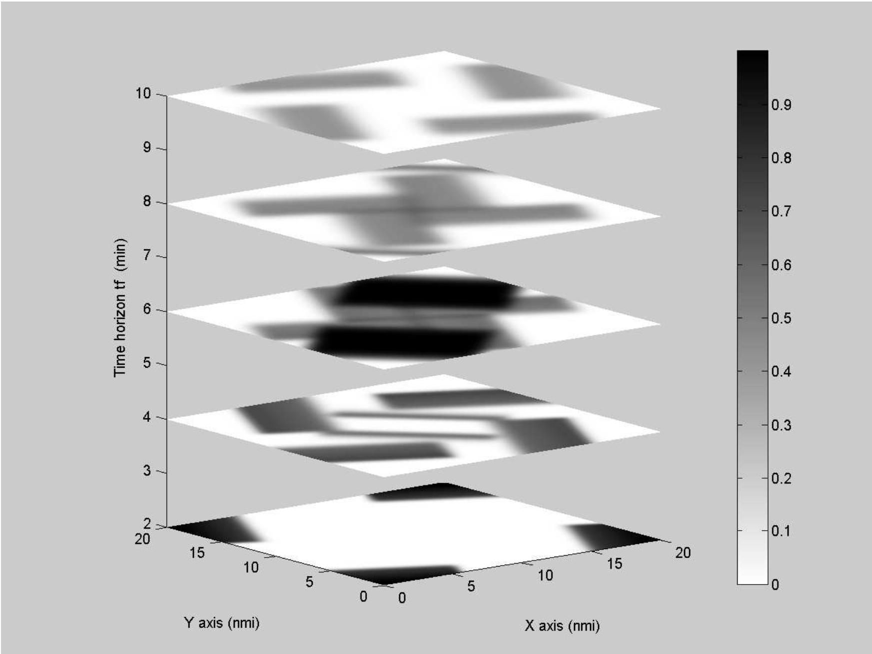

(a) Γ_1 probabilistic occupancy maps

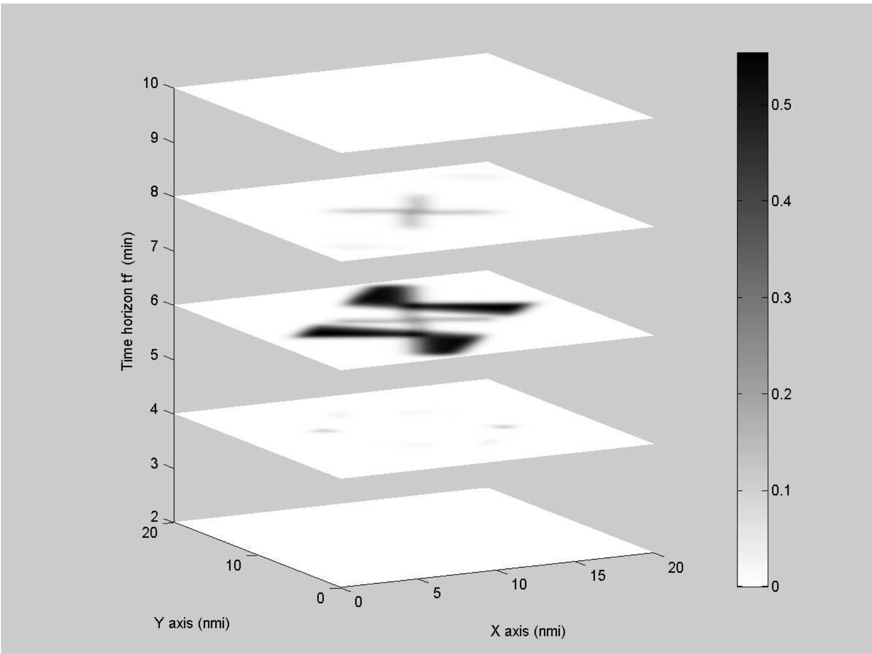

(b) Γ_2 probabilistic occupancy maps

Figure 10: Probabilistic occupancy maps over the XY plane corresponding to different time frames $[t_s, t_f]$ of length 2 min in the time horizon $[0, 10]$ min.

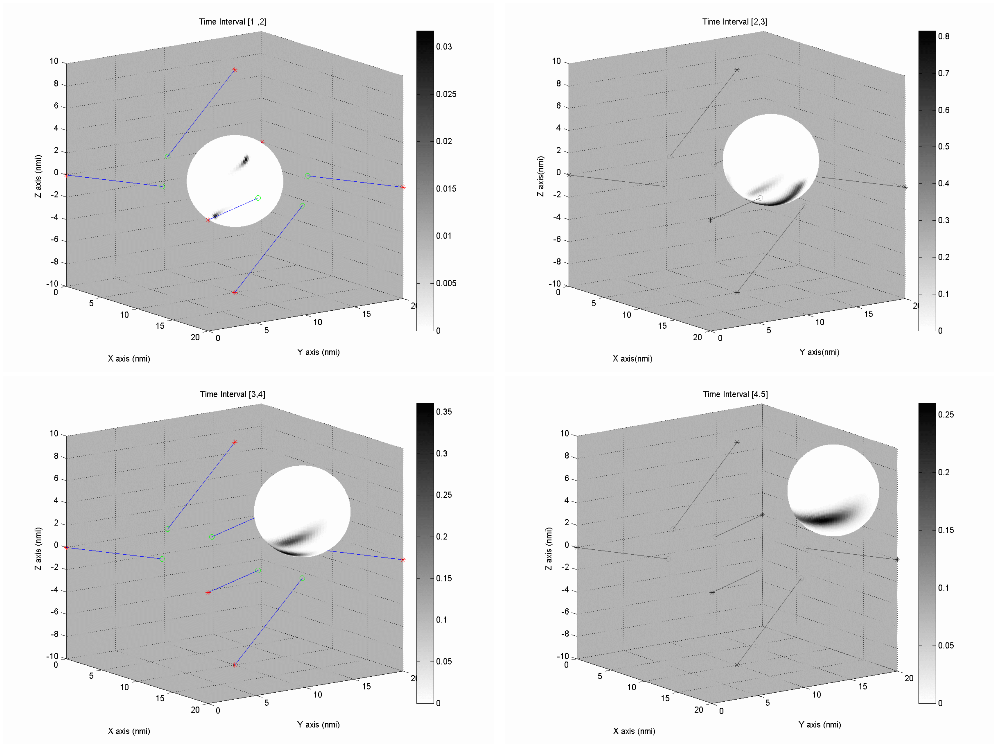

Figure 11: Complexity experienced by aircraft B entering an airspace region with other six aircraft as a function of its heading at a few points along its straight line trajectory.

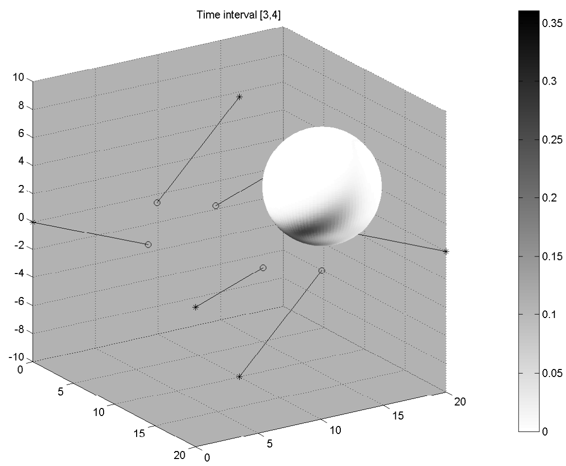

Figure 12: Complexity experienced by aircraft B as a function of its heading within the time frame [3,4] minutes when $\sigma_1^{A_i} = 1$ nmi $\cdot$ (min)$^{-1/2}$ and $\sigma_2^{A_i} = \sigma_3^{A_i} = 0.4$ nmi $\cdot$ (min)$^{-1/2}$.

Trajectory design:

Suppose that an aircraft B has to enter the airspace region $\mathcal{S}$ at time 0 and reach some destination position at time $\bar{t}$. The intended trajectory of the aircraft is a straight line traveled at constant velocity between its entry point and destination. However, this trajectory is not guaranteed to be of low-complexity due to the presence of other aircraft. Aircraft B can then choose a fixed number m of velocity changes at specified points in time $0 < t_1 < t_2 < \ldots < t_m < t_f$ to reduce the complexity along its trajectory. Note that the way points $X_1, X_2, \ldots, X_m$ at which aircraft B changes its velocity completely specify its nominal multi-legged trajectory. Since the flight time between successive way points is given, the velocity of aircraft B within each interval can be determined from the way points $X_1, X_2, \ldots, X_m$ and the starting and destination positions.

We seek to find an optimal trajectory in the sense that both the deviation from the intended trajectory and the complexity $\gamma_B(0)$ experienced by aircraft B within the flight time $[0, \bar{t}]$ ($\Delta = \bar{t}$) are minimized. We take the sum of the distances of the way points $X_1, X_2, \ldots, X_m$ from the intended trajectory as measure of the deviation d.

The complexity experienced by aircraft B along a multi-legged trajectory is not easy to compute since aircraft B does not have a constant velocity through out its flight, but only keeps its velocity constant during each interval $[t_i, t_{i+1}], i = 0, 1, \ldots, m$. However, we can over-approximate it by the sum of the complexities evaluated along the time intervals $[t_i, t_{i+1}]$ where aircraft B is flying at constant velocity v_i from X_i to X_{i+1} as suggested in Section 5.1.4 when dealing with the multi-legged nominal trajectory case.

The problem of finding a suitable trajectory is then formulated as that of minimizing the cost:

$$J := d + \lambda \hat{\gamma}_B(0), \tag{30}$$

which is a weighted sum of the deviation measure d and the over-approximation of the complexity measure $\hat{\gamma}_B(0)$. A higher value of the weighting coefficient $\lambda > 0$ attributes a greater priority to the low-complexity requirement, and results in a less conflict-prone trajectory for appropriately chosen size of the buffer zone.

In Figure 13, an encounter situation is shown, where some aircraft B enters an airspace region at time 0 and aims at reaching a destination position at time $\bar{t} = 10$, while keeping at some constant altitude. Four aircraft are already present in that region. Assume that aircraft B follows a level flight trajectory with one possible velocity change ($m = 1$) at $t_1 = 5$ out of a total flight time $\bar{t} = 10$.

Figure 13 shows the optimal trajectory of aircraft B obtained by minimizing the cost function (30) with $\lambda = 1500$, when $\sigma_1^{A_i} = 0.25$ nmi $\cdot$ (min)$^{-1/2}$ and $\sigma_2^{A_i} = \sigma_3^{A_i} = 0.2$ nmi $\cdot$ (min)$^{-1/2}$. The minimization was done using the MATLAB function *fmincon* and with the intended straight trajectory as the initial guess for the solution. The color map in Figure 13 represents the sum of the complexity measures within the time intervals $[0, 5]$ and $[5, 10]$ evaluated for different choices of the intermediate way point. The original intended trajectory is also plotted for comparison. It can be observed that the sum of the complexity measures along this trajectory is greater than that of the optimal one. A larger value of λ places more emphasis on the low-complexity

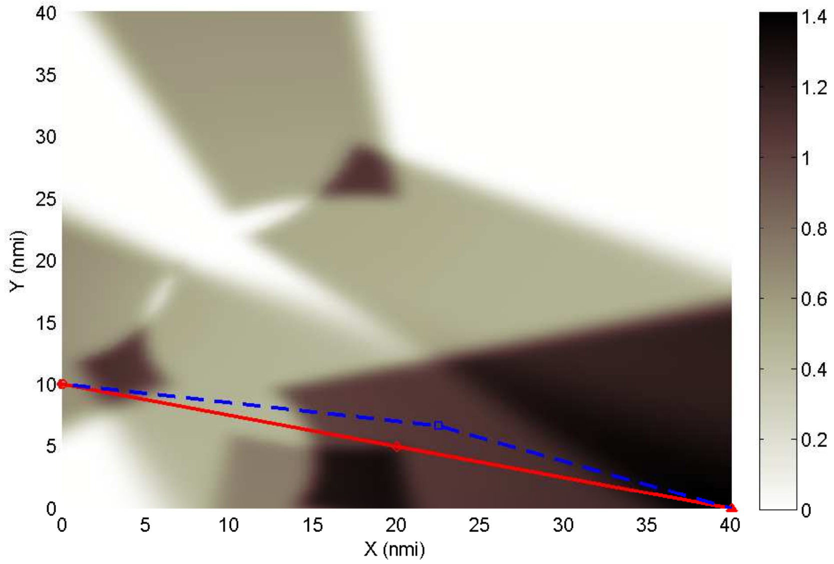

Figure 13: Originally intended trajectory (solid line) and optimal trajectory (dashed line) of aircraft B flying from the starting position on the left to the destination position on the right ($\lambda = 1500$). The color map in the background represents the complexity along aircraft B trajectory as a function of the intermediate way point position.

requirement and thus leads to more aggressive maneuvering.

5.2 A geometric approach to complexity evaluation

5.2.1 Introduction

In this section, we describe a complexity metric which could be used for the strategic trajectory management operations within the A^3 ConOps, as described in Chapter 2.

The metric was introduced in [9] and is built upon a simple idea: complexity at position x and time t depends on whether it would be convenient for an aircraft to be at that specific position x in that specific time t or not. The complexity metric should quantify how likely it is that the aircraft will be forced to tactically maneuver at that point, and, as such, it is a local measure.

5.2.2 Definition of local complexity

The local complexity at a point C takes into account all the aircraft inside a rotational ellipsoid $E(C)$ centered at C and with axis of rotation in vertical direction, whereas the contributions of aircraft outside the ellipsoid $E(C)$ are neglected.

More precisely, the value $M(C, t)$ of the complexity metric at point C and time t is defined as the sum of the contributions m_i's of all aircraft i whose intended position

$A_i(t)$ at time t lies inside the ellipsoid $E(C)$:

$$M(C,t) = \sum_{\{i:A_i(t)\in E(C)\}} m_i(C,t) \tag{31}$$

In turn, $m_i(C,t)$ is determined by the intended position and the actual direction of flight (track angle, inertial flight path angle) of aircraft i at time t, as follows:

$$m_i(C,t) = \log_2\left(1 + \frac{|A_iP_i|}{|CP_i|}\frac{1}{1+e^{k(\frac{\alpha_i}{\pi}-0.5)}}\right) \tag{32}$$

where point P_i is given by the intersection of semi-axis CA_i with the boundary of the ellipsoid $E(C)$ and α_i is the angle between the actual direction of flight and vector A_iC (see Figure 14). Dependence of A_i, P_i and α_i from t is omitted for brevity.

The angle α_i is measured in radians and takes values in $[0,\pi]$ ($\alpha_i = 0$ means that the aircraft is heading towards C, and $\alpha_i = \pi$ that it is moving away from C).

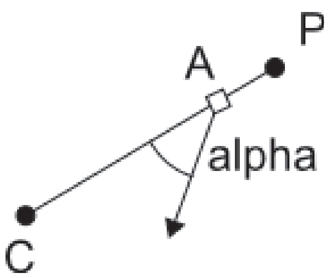

Figure 14: Metric definition scheme.

In formula (32), the distance-based component $\frac{|A_iP_i|}{|CP_i|}$ aims at emphasizing the influence of the aircraft that are closer to the ellipsoid center C, while the angle-based component $\frac{1}{1+e^{k(\frac{\alpha_i}{\pi}-0.5)}}$ takes into account the extent to which the aircraft is heading towards the point C. The direction of the flight is considered in a nonlinear way using the classic sigmoidal function. The range of both the distance-based and angle-based component, as well as of the single aircraft contribution to the local complexity, is $[0,1]$.

Also, the local complexity metric possesses the following properties:

- the contribution of an aircraft to the complexity is continuous as a function of the space; and
- the metric is additive with respect to contributing aircraft.

Due to these two properties, the measure is relatively robust to possible local deviations of the aircraft from their predicted trajectory.

5.2.3 Complexity maps

4D complexity maps can be generated based on the proposed local measure of complexity in a given airspace region. To this purpose the metric is computed on a regular spatial grid, using snapshots of (predicted) traffic throughout time at regular sampled times.

To the purpose of obtaining a compact representation of the 4D complexity maps, their sampled version on a rectangular grid is filtered using a threshold (or multiple thresholds, if desired). A segmentation algorithm is then applied so that it is clear how many components (that is, 4D areas of complexity) are present. Each component is then simplified as much as possible, so that clearly defined objects are obtained. This process shall reflect the requirements of the applications: for computation of the optimal trajectories, communication, displaying to a pilot/controller, etc., it is necessary that the areas are easily represented. Components that are too small can be omitted; those that are close to each other can be merged; those with "holes" inside can be filled; those that are complicated to describe can for example be over-approximated by a convex set.

A lateral view of the 3D spatial complexity map of one aircraft is shown in Figure 15. It illustrates well the contribution of the direction of the flight to the local complexity and the related added value with respect to the simple traffic density calculation, which does not account for the aircraft directivity and velocity, and, hence, does not take into consideration any geometrical factor related to the air traffic evolution.

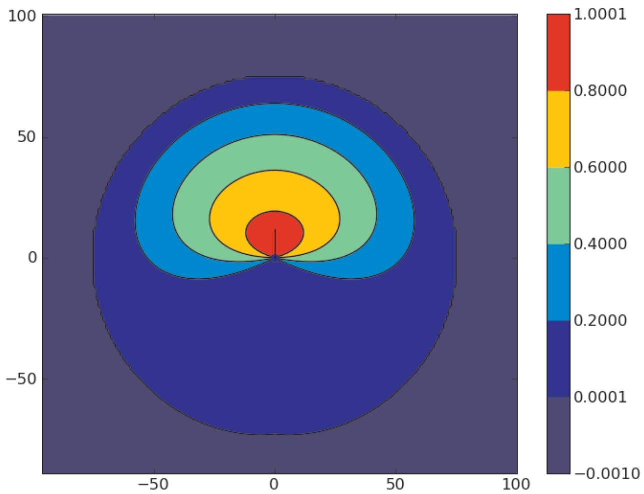

Figure 15: Complexity map due to a single aircraft (lateral view).

As in the probabilistic approach, the computation effort involved in complexity evaluation at each grid point scales linearly with the number of aircraft. Indeed, when building the complexity map, one does not have to explicitly evaluate the interactions between aircraft (such as converging or diverging tendencies), which will eventually cause an exponential growth of the effort. Nevertheless, such an interaction is still inherently present: if two aircraft are converging, there is certainly a point in the grid close to both of them and in the direction of their flight, which will take high complexity values. In the same vein, diverging aircraft will not contribute together to high complexity values in any grid point.

Example 1 (complexity maps) Figure 16 to Figure 19 show the evolution of a complexity of an air traffic situation at times 300 seconds, 600 seconds, 900 seconds and 1200 seconds after the "ownship" left from the position [0,0]. This example uses a random traffic with approximately 50 aircraft with two mild crossing flows.

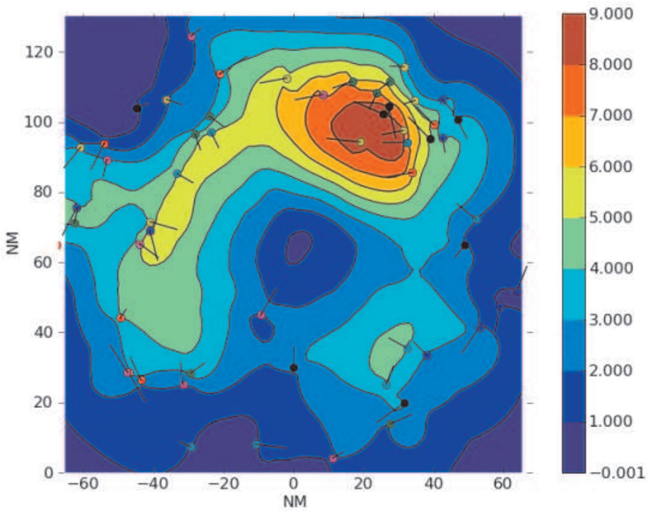

Figure 16: Complexity map of an air traffic example - time 300 s.

The angle-based component of the metric can be shaped through the parameter k. In this example, we adopted the value $k = 12$. For the horizontal semi-axis of the ellipsoid $E(C)$, the value 40 nmi (about 5 minutes of the en-route flight) was used. For the vertical semi-axis of the ellipsoid $E(C)$ the value of 10 000 ft was considered (10 Flight Levels).

The spatial gridding was 5 nmi on the horizontal plane and 1600 ft vertically, whereas a sampling time period of 60 seconds was adopted.

The optimal choice of numerical parameters is of course tightly connected to the realistic parameters of the air traffic system and detailed operational requirements. So the values used in the example are based on an initial estimation and first simple validation.

5.2.4 Setting the thresholds to identify complex areas-to-avoid

The complexity map itself provides only relative information about the air traffic complexity: it shows areas with higher or lower complexity, but does not tell anything about feasibility (in terms of flying through) of these places. In other words, we need thresh-

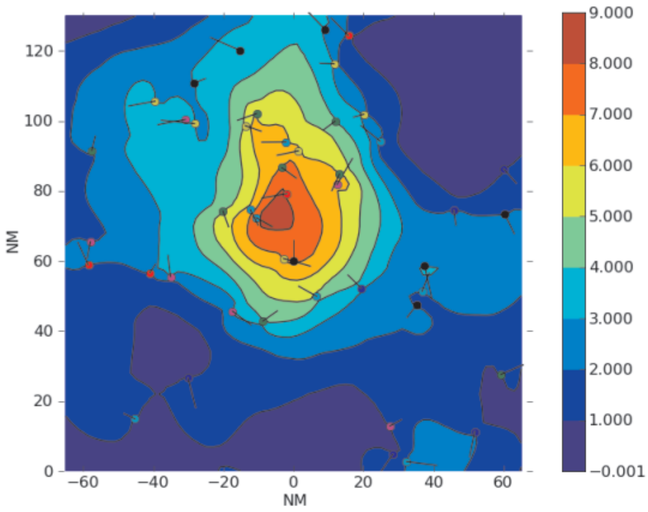

Figure 17: Complexity map of an air traffic example - time 600 s.

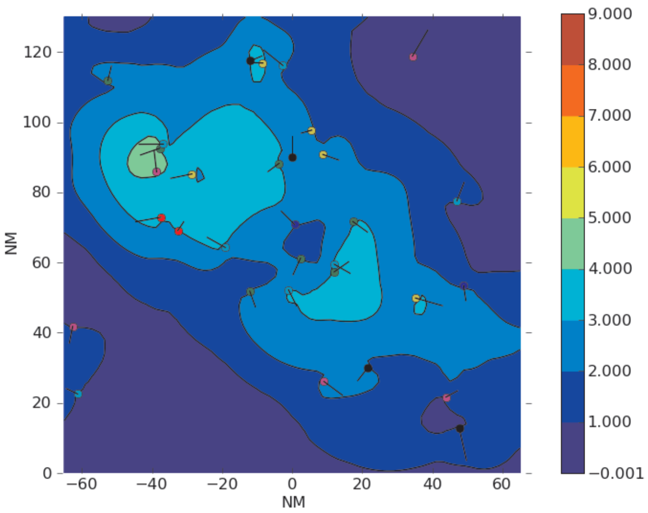

Figure 18: Complexity map of an air traffic example - time 900 s.

old value(s) that would help us distinguish between areas which should be avoided and areas suitable for flight (from air traffic perspective).

For a distributed trajectory optimization we propose application of two thresholds: a hard threshold and a soft threshold (see an example in Figure 20). Their intended use is as follows: The hard limit is the complexity value that should not be exceeded. The soft limit is the hard limit decreased by 1. It can be ignored during an assessment of a planned path, however should be taken into account if re-planning takes place. Note

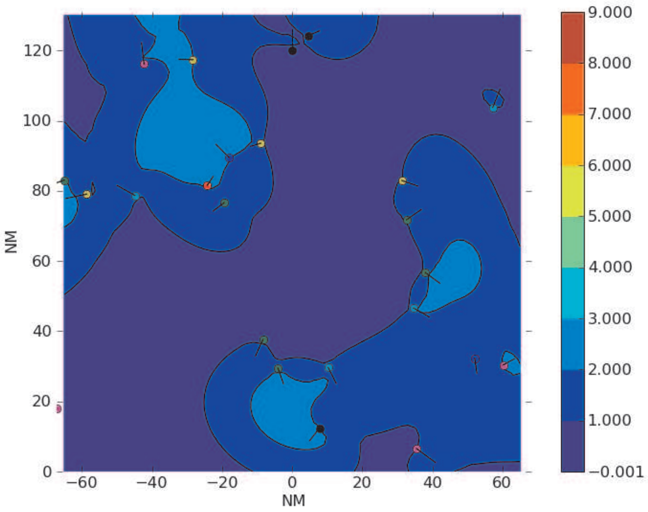

Figure 19: Complexity map of an air traffic example - time 1200 s.

that the complexity is computed based on all the aircraft involved. So if a pilot of one such aircraft finds out that his/her plane (ownship) is going to fly through a complexity area given by the soft limit, but not through an area given by the hard limit, he/she can expect that the complexity will not exceed the hard limit. On the other hand if a new trajectory is designed (for example, a bypass around an area given by the hard limit), the new path should avoid the soft limit borders as well.

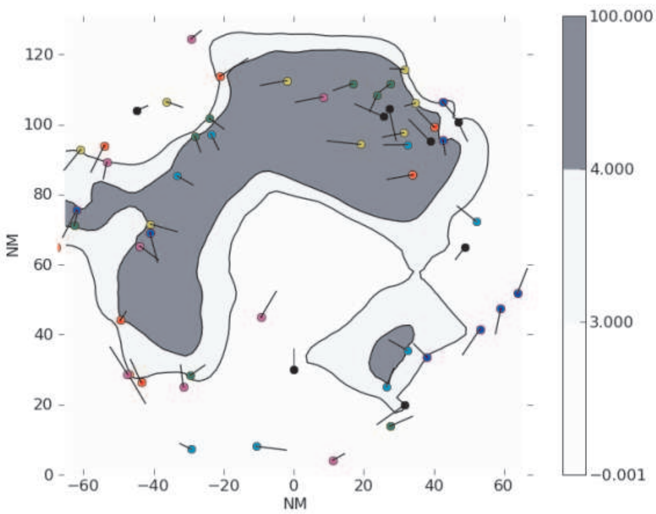

Figure 20: Complexity map of an air traffic example - time 300 s. Soft threshold (value 3) and hard threshold (value 4) are applied.

The reason is that the complexity far from the original flight path was computed with little or no contribution from the ownship, but after a flight path change, the contribution of the ownship would be equal to one exactly on the new path, and close to this number in the near neighborhood. So, if the new flight path is planned in the areas with complexity less than the soft limit, it is certain that after that change the complexity there will not exceed the hard limit.

The right value of the hard threshold may depend mainly on the character, requirements and expectations of each user, and should be a result of deep analysis. Here we only provide a glimpse into the complexity values meaning through some experiment. We simulated one thousand instances of a random traffic (with two main crossing flows of traffic of moderate intensity) at a square of 130 nmi x 130 nmi. The traffic was not de-conflicted in advance by any strategic flow management, and conflicts occurred now and then. For a selected ownship travelling through the area, the ratio of discrete time instances with a conflict (loss of separation) to the total number of time instances, was evaluated for each complexity interval of length 1. The results are shown in Figure 21.

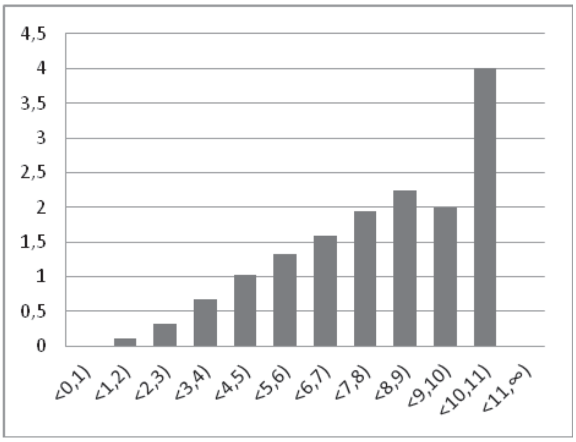

Figure 21: Conflict ratio (vertical axis) vs. complexity range (horizontal axis).

The first complexity interval is empty. This is due to the fact that the ownship itself increases the complexity value by one, as the complexity is measured exactly in the ownship's position in this experiment. All measured complexity values were lower than 11, so the last column is also empty. The penultimate column represents only one case: a time instance when the ownship has conflicts with 4 other aircraft at once, but generally this is also a rare situation. The rest of the columns, however, can tell a little about the relation between the complexity measure and conflicts experienced at the same time: For example, if we want the probability of conflicts to be around 0.5, the aircraft should avoid areas with complexity higher than 3 or 4 (see the fourth most left column). Nevertheless, finer complexity categorization would be necessary in order to find the right balance between conflicts and complexity areas size (usually, the lower complexity threshold, the larger the area determined by the threshold value).

5.2.5 Map representation for onboard trajectory management

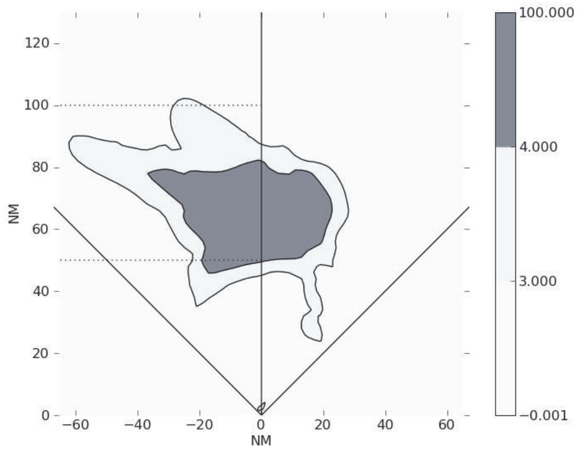

Figure 22: A subjective view on the traffic complexity from the single aircraft perspective. The intended flight path goes through a hard threshold area, therefore re-planning is needed.

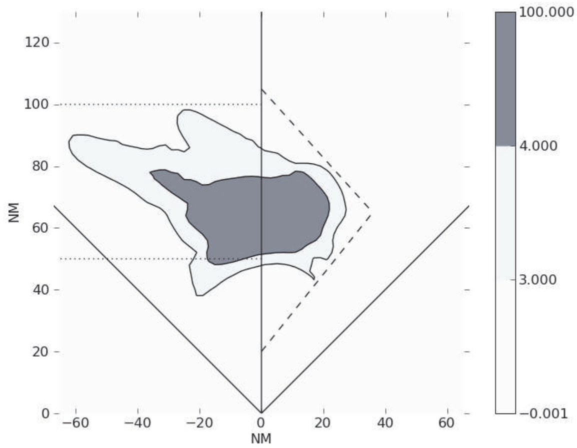

Figure 23: New trajectory (dashed line) avoiding the complex areas.

In the previous part, we have already outlined how thresholds can be set and used for the trajectory optimization application. In the case of an onboard application only the resulting 4D complexity areas are sent to the aircraft. Still there can be many of them, and their predicted evolution in time can be rather complicated (see the example in the previous section). Note, however, that the only relevant information for the crew or the onboard trajectory planning system is that related to those times and positions that can be actually reached by the aircraft. For instance, complexity values at positions that are far from the current aircraft position are not of interest. Thus it would be waste of communication effort to transmit and process such information. Instead, according to the expected speed profile of the aircraft, only a 2D cross section (the complexity at different grid points is evaluated for the time when this point could be reached by own aircraft) through the 4D grid can be used, providing the subjective view of the expected complexity evolution to be experienced by the aircraft. Such a subjective 2D view for the ownship from our example (see Figure 16 to Figure 19) is shown in Figure 22. The main axis shows the intended flight path of the ownship. Note that the subjective view not only reveals all the details of the evolution of complexity from the ownship's subjective perspective, but - if generated without the ownship's contribution (see Figure 23) - also helps to decide which way to go around an area of high complexity.

5.3 Comparative analysis

In this section we perform a comparative analysis of the two novel methods for complexity evaluation described in this chapter, in view of the airborne self separation application.

5.3.1 Features relevant to the airborne self separation application

The probabilistic and geometric approaches to complexity evaluation described in Sections 5.1 and 5.2 have the the following characteristics:

1. they are control-independent, in that complexity is evaluated without making reference to the way the traffic is controlled and only based on the aircraft (predicted) trajectories;
2. they account for the aircraft density and the traffic dynamics;
3. they can be applied to assess complexity on either a mid term or a long term horizon, depending on the look-ahead time horizon of the predicted trajectory;
4. they can provide a 4D map of complexity, based on which high complexity areas-to-avoid can be identified;
5. the contribution of each single aircraft to complexity can be computed in isolation and then combined with that of the other aircraft.

A key difference is that uncertainty in the future aircraft position is accounted for when evaluating complexity according to the probabilistic approach, whereas the geometric approach relies on the nominal aircraft trajectory for complexity evaluation.

Table 2 summarizes the characteristics of the two methods with reference to the features that were identified as relevant to airborne self separation in Section 2.3. Both methods satisfy the desired properties, the only issue being the high computational load and

Table 2: Characteristics of the novel methods for complexity evaluation.

metric	**input data**	**method**	**accounting for traffic dynamics**	**sector-independent**	**look-ahead time horizon**	**control-independent**	**output form**	**computational load**
probabilistic approach	aircraft timed trajectories	probabilistic occupancy within an ellipsoidal buffer region	yes	yes	short/mid/long term	yes	4D map/scalar-valued function (probabilistic occupancy as a function of time and airspace position/timed aircraft trajectory)	high for the 4D map due to gridding, moderate for the scalar-valued function
geometric approach	aircraft timed trajectories	weighted density within an ellipsoidal buffer region, weights depend on flight direction and position relative to the center	yes	yes	short/mid/long term	yes	4D map (weighted local density as a function of time and airspace position)	high due to gridding

memory requirements involved in the construction and update of the 4D maps, which is only partly alleviated by the feature described at point 5.

According to the A^3 ConOps described in A^3 ConOps described in Deliverable 1.3, [13], complexity maps for trajectory management purposes will be computed on the ground, where higher computational power is available, and only relevant information in terms of areas-to-avoid will be transmitted onboard. Nevertheless, parallelized implementations and some adaptive gridding scheme using a finer gridding of the airspace in those regions that are close to the aircraft nominal trajectories can be adopted to reduce the computational requirements.

In the probabilistic approach to complexity evaluation, a single-aircraft complexity metric is also introduced. Whereas the construction of the global complexity map involves 4D (time and 3D space) gridding, computations of the single-aircraft complexity metric are confined to the aircraft nominal path and involve only one-dimensional gridding. As such they are better suited for onboard implementation.

5.3.2 Capability of detecting traffic configurations that are difficult to control

We now assess the performance of the two methods for in terms of capability of the corresponding metrics of identifying those air traffic configurations that are difficult to control. More specifically, we analyze the correlation between collision risk and a scalar measure of complexity in a scenario where control is delegated to the aircraft.

The study was conducted jointly with WP7 of the iFly project. Within WP7, complexity measures could be used to identify the air traffic configurations that are more likely to lead to a collision in order to speed-up the IPS method for estimating the collision risk in a self separating aircraft scenario, [7].

The standard Monte Carlo approach to probability estimation requires a number of simulations that scales as the inverse of the probability to be estimated. This makes it impracticable for estimating the probability of a rare event such as a collision, and calls for ad-hoc solutions. In the IPS method, the number of simulations to estimate the collision risk is significantly reduced by representing the collision risk as the product of the conditional probabilities of an increasing sequence of conditionally not-so-rare events. In this sequence, the aircraft get at progressively smaller distances one from the other, reaching nested levels of proximity. Each of these conditional probabilities, e.g., the probability of reaching level $k + 1$ given that level k has been reached, is estimated by simulating in parallel several copies of the system. Each copy represents a *particle* and evolves according to the system dynamics. Re-initialization is performed at every level k by re-sampling the particles according to the empirical distribution as determined by the particles that have reached such a level.

Although the IPS approach to collision risk estimation outperforms the standard Monte Carlo approach, it still poses very high requirements on the availability of dynamic computer memory and simulation time. The idea jointly developed with WP7 is to improve the performance of the IPS algorithm by selecting among the initial aircraft configurations those that are more prone to lead to a collision and propagating through the system dynamics only the corresponding particles. These configurations are identified based on the value taken by some complexity metric. This idea is inspired by the variance reduction technique known in the Monte Carlo simulation literature as *importance sampling*, where samples are extracted according to a "biased" distribution that is higher in those regions making the most important contribution to the quantity to be estimated, and the outcome of the simulations is then re-scaled to get an unbiased estimate. More details on the resulting integrated approach are reported in [61].

We run our test on a Stochastically and Dynamically Coloured Petri Net (SDCPN) simulator of the AMFF [53], which was developed to study the introduction of autonomous free flight operation in Mediterranean airspace. The SDCPN model is composed of interconnected Local Petri Nets modelling each agent involved in the process (e.g., aircraft, pilot, navigation and surveillance equipment) and is described in details in [7].

The IPS algorithm was applied to an hypothetical AMFF air traffic scenario where one aircraft is flying through a virtual infinite airspace of randomly distributed aircraft. The traffic density was set equal to 2.5 times the density of 0.0032 aircraft per nmi^3 experienced on 23rd July 1999 in an en-route busy area near Frankfurt. To reproduce such a density, the airspace was divided into packed containers, each one having a length of 40 nmi, a width of 40 nmi, and a height of 3900 feet and containing 8 aircraft. The virtually infinite airspace is build according to the following procedure. A set of 8 aircraft ($i = 1, 2, \dots, 8$) flying at arbitrary position and in arbitrary direction at a ground speed of about 466 nmi/h is generated first in a container. Duplicates of this container are then piled on top and next to each other (9 containers in the x and y-directions and 11 in z-direction). Note that, since the aircraft within each container behave the same, in principle an aircraft can experience a conflict with its own copy in a neighboring container.

The aim is to estimate the probability of collision of aircraft $i = 1$ in the central container with any of the other aircraft per unit time of flying. By running the IPS algorithm ten times over 15 minutes the collision probability per unit time of flying can be estimated. The number of initial particles per IPS simulation run is 10000, each one corresponding to an aircraft initial configuration. 8 nested levels of proximity are considered as detailed in [7]. The initial aircraft configurations that are more prone to a collision are those with a larger number of regenerated samples hitting level 8. The results obtained by applying the standard IPS method are reported in Table 3.

The capability of a method for complexity evaluation to detect critical encounter configurations can be assesses by evaluating the speed-up factor achieved in the IPS algorithm by selecting the particles to be propagated through the system dynamics based on the corresponding complexity value.

We start by illustrating the results obtained with the approach to complexity evaluation

Table 3: Results obtained through the standard IPS.

run	**risk estimate**
1	$7.28 \cdot 10^{-5}$
2	$8.83 \cdot 10^{-5}$
3	$3.54 \cdot 10^{-5}$
4	$1.03 \cdot 10^{-4}$
5	$1.22 \cdot 10^{-5}$
6	$7.21 \cdot 10^{-5}$
7	$2.66 \cdot 10^{-6}$
8	$3.94 \cdot 10^{-5}$
9	$1.41 \cdot 10^{-4}$
10	$8.03 \cdot 10^{-6}$
mean	$5.75 \cdot 10^{-5}$

presented in Section 5.1.

Performance of the probabilistic approach to complexity evaluation

The single-aircraft complexity measure $\gamma_B(0)$ defined in (10) with $\Delta = 15$ minutes was used with aircraft B representing the aircraft in the central box for which collision risk is estimated.

The spectral densities of the uncertainty affecting the future aircraft position were set equal to $\sigma_1^{A_i} = 0.25$ nmi $\cdot$ (min)$^{-1/2}$ in the along track direction, and $\sigma_2^{A_i} = \sigma_3^{A_i} = 0.2$ nmi$\cdot$(min)$^{-1/2}$ in the cross track directions. The parameters r_h and r_v defining the ellipsoidal buffer region surrounding aircraft B were set equal to $r_h = r_v = 0.05$ nmi to reproduce a condition of collision.

The value taken by $\gamma_B(0)$ is used to decide whether some given airspace configuration has to be propagated through the system dynamics in the IPS algorithm or not. In the former case we call the configuration a *selected particle*.

Figure 24 refers to run number 1 and plots the diagram of the probability that $\gamma_B(0)$ exceeds some threshold as a function of the threshold value. Similar plots can be obtained for the other runs. Additional information is provided by the histograms of $\gamma_B(0)$ for the particles hitting the conflict levels from 1 to 8 (see the plots in Figure 25 for run 1).

In the IPS algorithm with importance sampling, the initial particles for which $\gamma_B(0)$ is lower that some threshold are discarded and the IPS algorithm is run on the selected particles only. The impact of this procedure in terms of reduction of the number of particles to simulate and degradation of the IPS collision risk estimate can be evaluated

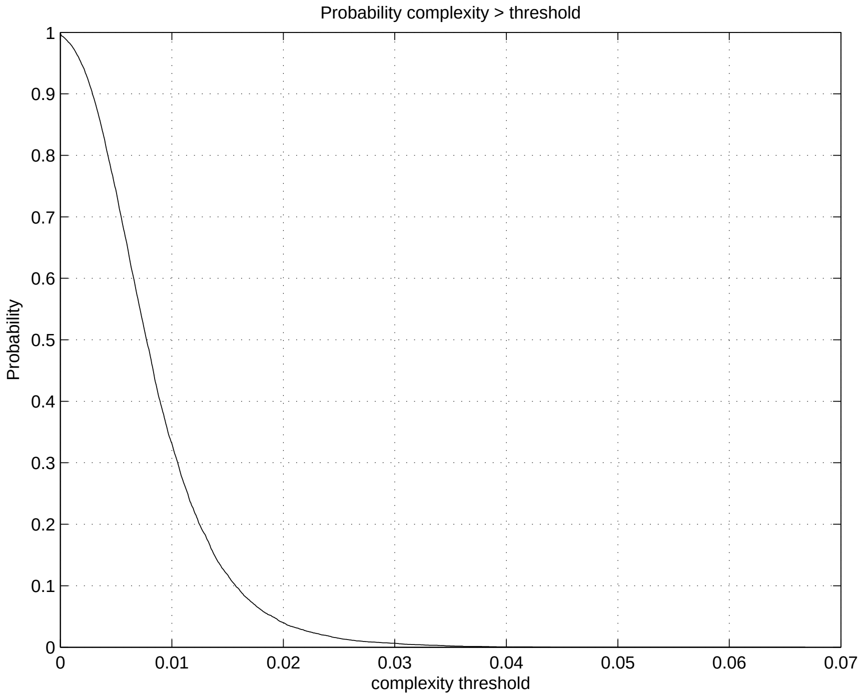

Figure 24: Diagram of the probability that $\gamma_B(0)$ exceeds the threshold as a function of the threshold value (run number 1).

in each run through the following quantity

$$\text{gain} := \frac{\frac{\text{original number of particles}}{\text{number of selected particles}}}{\frac{\text{risk estimate with all particles}}{\text{risk estimate with the selected particles}}}.$$

The overall gain over the 10 runs of the IPS algorithm can be computed through the same formula applied to average quantities.

Increasing values of the threshold (0.010, 0.015, 0.020, 0.025, 0.030 and 0.035) have been considered in our experiments (see Tables 4-9).

Obviously, as the threshold increases, the number of selected particles decreases. This has the beneficial effect of reducing the computational effort in the IPS algorithm, but may lead to an excessive impoverishment of the set of initial particles and cause the collision risk estimate to be zero (i.e., no particle reaches the final level 8). In view of this consideration, the threshold value 0.03 (and, hence, also 0.035) can be considered too large since the collision risk estimate is zero in more than 50% of the runs. The speed-up factor for the threshold values smaller than 0.03 can be estimated by re-scaling the overall gain factor with the fraction of runs that correspond to a nonzero estimated risk. The larger speed-up factor turns out to be 15.30 and corresponds to the threshold value 0.025.

Table 4: Results obtained with $\gamma_B(0)$ when the threshold is set equal to 0.010.

run	**selected particles**	**estimate**	**gain**
1	3317	$5.84 \cdot 10^{-5}$	2.4
2	3269	$6.38 \cdot 10^{-5}$	2.2
3	3235	$1.20 \cdot 10^{-5}$	1.0
4	3246	$9.24 \cdot 10^{-5}$	2.8
5	3271	$5.90 \cdot 10^{-7}$	0.1
6	3265	$1.39 \cdot 10^{-5}$	0.6
7	3215	0.0	0.0
8	3186	$9.79 \cdot 10^{-6}$	0.8
9	3256	$1.24 \cdot 10^{-4}$	2.7
10	3201	$2.33 \cdot 10^{-7}$	0.1
mean	3246	$3.75 \cdot 10^{-5}$	1.3

overall gain: $(10000/3246)/(5.75 \cdot 10^{-5}/3.75 \cdot 10^{-5}) = 2.0$

Table 5: Results obtained with $\gamma_B(0)$ when the threshold is set equal to 0.015.

run	**selected particles**	**estimate**	**gain**
1	1177	$4.11 \cdot 10^{-5}$	4.8
2	1157	$3.40 \cdot 10^{-5}$	3.3
3	1135	$1.20 \cdot 10^{-5}$	3.0
4	1136	$9.24 \cdot 10^{-5}$	7.9
5	1092	$5.90 \cdot 10^{-7}$	0.4
6	1139	$1.01 \cdot 10^{-5}$	1.2
7	1087	0.0	0.0
8	1093	$9.79 \cdot 10^{-6}$	2.3
9	1127	$7.73 \cdot 10^{-5}$	4.9
10	1121	0.0	0.0
mean	1126	$2.77 \cdot 10^{-5}$	2.8

overall gain: $(10000/1126)/(5.75 \cdot 10^{-5}/2.77 \cdot 10^{-5}) = 4.3$

Table 6: Results obtained with $\gamma_B(0)$ when the threshold is set equal to 0.020.

run	**selected particles**	**estimate**	**gain**
1	398	$7.46 \cdot 10^{-8}$	0.0
2	415	$3.40 \cdot 10^{-5}$	9.3
3	385	$1.20 \cdot 10^{-5}$	8.8
4	368	$9.20 \cdot 10^{-5}$	24.3
5	347	$5.90 \cdot 10^{-7}$	1.4
6	392	0.0	0.0
7	358	0.0	0.0
8	377	0.0	0.0
9	386	$7.73 \cdot 10^{-5}$	14.2
10	382	0.0	0.0
mean	381	$2.16 \cdot 10^{-5}$	5.8

overall gain: $(10000/381)/(5.75 \cdot 10^{-5}/2.16 \cdot 10^{-5}) = 9.9$

Table 7: Results obtained with $\gamma_B(0)$ when the threshold is set equal to 0.025.

run	**selected particles**	**estimate**	**gain**
1	146	$7.46 \cdot 10^{-8}$	0.1
2	147	$3.39 \cdot 10^{-5}$	26.1
3	142	$2.45 \cdot 10^{-6}$	4.9
4	143	$9.20 \cdot 10^{-5}$	62.6
5	133	$5.90 \cdot 10^{-7}$	3.6
6	133	0.0	0.0
7	142	0.0	0.0
8	134	0.0	0.0
9	146	$7.73 \cdot 10^{-5}$	37.6
10	143	0.0	0.0
mean	141	$2.06 \cdot 10^{-5}$	13.5

overall gain: $(10000/141)/(5.75 \cdot 10^{-5}/2.06 \cdot 10^{-5}) = 25.5$

Table 8: Results obtained with $\gamma_B(0)$ when the threshold is set equal to 0.030.

run	**selected particles**	**estimate**	**gain**
1	65	$7.46 \cdot 10^{-8}$	0.2
2	56	$3.39 \cdot 10^{-5}$	68.5
3	54	$2.45 \cdot 10^{-6}$	12.8
4	50	$9.20 \cdot 10^{-5}$	179.1
5	44	0.0	0.0
6	57	0.0	0.0
7	46	0.0	0.0
8	55	0.0	0.0
9	72	0.0	0.0
10	48	0.0	0.0
mean	55	$1.28 \cdot 10^{-5}$	26.1

overall gain: $(10000/48)/(5.75 \cdot 10^{-5}/1.28 \cdot 10^{-5}) = 40.9$

Table 9: Results obtained with $\gamma_B(0)$ when the threshold is set equal to 0.035.

run	**selected particles**	**estimate**	**gain**
1	21	$7.46 \cdot 10^{-8}$	0.5
2	19	0.0	0.0
3	24	$2.45 \cdot 10^{-6}$	28.8
4	23	$9.20 \cdot 10^{-5}$	389.4
5	17	0.0	0.0
6	26	0.0	0.0
7	18	0.0	0.0
8	16	0.0	0.0
9	26	0.0	0.0
10	14	0.0	0.0
mean	20	$9.45 \cdot 10^{-6}$	41.9

overall gain: $(10000/20)/(5.75 \cdot 10^{-5}/9.45 \cdot 10^{-6}) = 81$

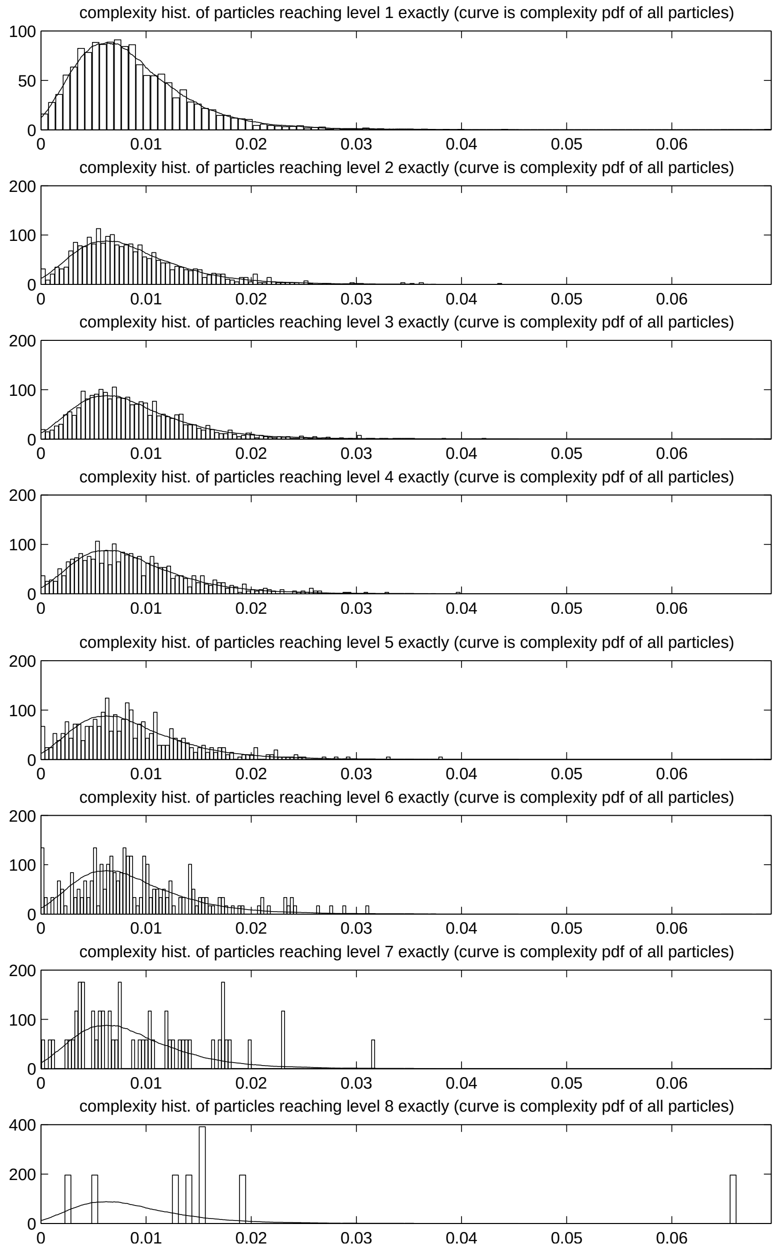

Figure 25: Histograms of $\gamma_B(0)$ for the particles hitting the conflict levels from 1 to 8 (run number 1).

Performance of the geometric approach to complexity evaluation

The complexity metric (31) is computed along the nominal trajectory of the aircraft in the central box, say $x_B(t)$, for which collision risk is estimated. Complexity is evaluated every $\Delta = 10$ seconds and the largest value along the 15 minutes time horizon

$$M_{\max} := \max_{k \in \{0,1,\ldots,15 \cdot 6\}} M(x_B(k\Delta), k\Delta)$$

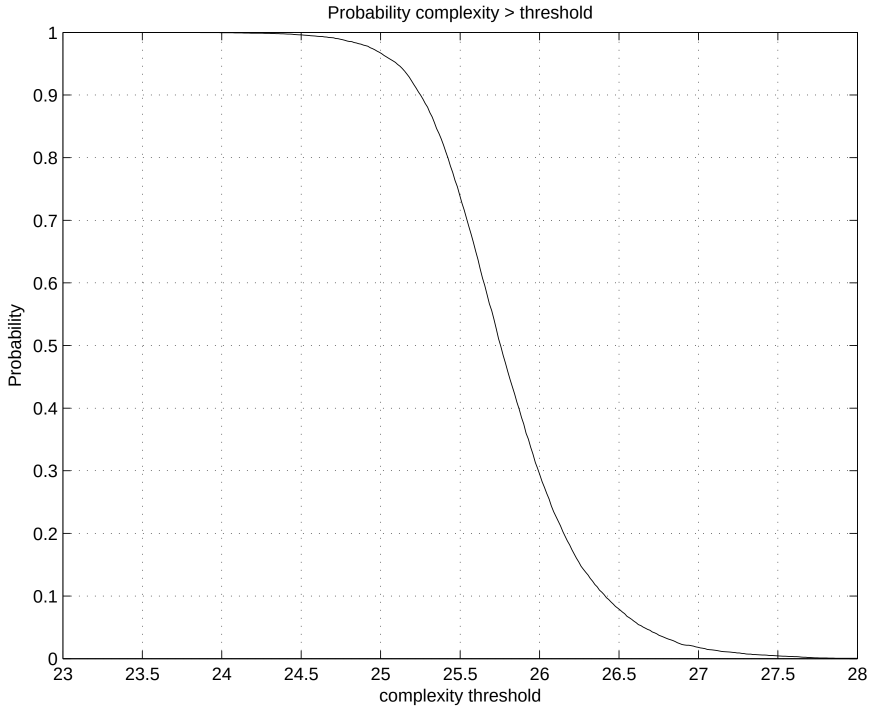

Figure 26: Diagram of the probability that complexity M_{max} exceeds the threshold as a function of the threshold value (run number 1).

is used to identify the particles to be propagated in the IPS algorithm with importance sampling.

The semi-axes of the ellipsoid entering the complexity measure (31) are set equal to 100 km in the horizontal plane and to 3 km in the vertical direction, whereas $k = 12$.

Figure 26 refers to run number 1 and plots the diagram of the probability that M_{max} exceeds some threshold as a function of the threshold value. Similar plots can be obtained for the other runs. Additional information is provided by the histograms of M_{max} for the particles hitting the conflict levels from 1 to 8 (see the plots in Figure 27 for run 1).

Increasing values of the threshold (26.00, 26.25, 26.50, and 26.75) have been considered in our experiments. Results are reported in Tables 10-13.

In this case, threshold values larger than 26.25 can be considered too large since the collision risk estimate is zero in more than 50% of the runs. The speed-up factor for the threshold values 26.00 and 26.25 can be estimated by re-scaling the overall gain factor with the fraction of runs that correspond to a nonzero estimated risk. The larger speed-up factor is 1.05 and corresponds to the threshold value 26.00.

Table 10: Results obtained with $M_{\max}$ when the threshold is set equal to 26.00.

run	**selected particles**	**estimate**	**gain**
1	2953	$7.28 \cdot 10^{-5}$	2.7
2	2920	$2.29 \cdot 10^{-6}$	0.1
3	2903	$1.11 \cdot 10^{-5}$	1.1
4	3080	$9.22 \cdot 10^{-5}$	2.9
5	2992	0	0.0
6	2982	$1.01 \cdot 10^{-5}$	0.5
7	2969	0	0.0
8	2959	0	0.0
9	2907	$7.77 \cdot 10^{-5}$	1.9
10	2976	$4.82 \cdot 10^{-6}$	2.0
mean	2964	$2.57 \cdot 10^{-5}$	1.1

mean gain: $(10000/2964)/(5.75 \cdot 10^{-5}/2.57 \cdot 10^{-5}) = 1.5$

Table 11: Results obtained with $M_{\max}$ when the threshold is set equal to 26.25.

run	**selected particles**	**estimate**	**gain**
1	1530	$5.74 \cdot 10^{-5}$	5.2
2	1556	$2.29 \cdot 10^{-6}$	0.2
3	1496	$9.37 \cdot 10^{-6}$	1.8
4	1637	$9.22 \cdot 10^{-5}$	5.5
5	1555	0	0.0
6	1557	$3.94 \cdot 10^{-6}$	0.4
7	1554	0	0.0
8	1541	0	0.0
9	1498	$3.89 \cdot 10^{-7}$	0.0
10	1545	0	0.0
mean	1547	$1.66 \cdot 10^{-5}$	1.3

overall gain: $(10000/1547)/(5.75 \cdot 10^{-5}/1.66 \cdot 10^{-5}) = 1.3$

Table 12: Results obtained with $M_{\max}$ when the threshold is set equal to 26.50.

run	**selected particles**	**estimate**	**gain**
1	795	$5.74 \cdot 10^{-5}$	9.9
2	784	$2.29 \cdot 10^{-6}$	0.3
3	726	0	0.0
4	793	$9.22 \cdot 10^{-5}$	11.3
5	765	0	0.0
6	785	$9.62 \cdot 10^{-8}$	0.0
7	791	0.0	0.0
8	789	0	0.0
9	760	0	0.0
10	754	0	0.0
mean	774	$1.52 \cdot 10^{-5}$	2.2

overall gain: $(10000/774)/(5.75 \cdot 10^{-5}/1.52 \cdot 10^{-5}) = 3.5$

Table 13: Results obtained with $M_{\max}$ when the threshold is set equal to 26.75.

run	**selected particles**	**estimate**	**gain**
1	376	0	0.0
2	374	0	0.0
3	343	0	0.0
4	380	$9.20 \cdot 10^{-5}$	23.6.6
5	365	0	0.0
6	406	$9.62 \cdot 10^{-8}$	0.0
7	379	0	0.0
8	381	0	0.0
9	374	0	0.0
10	334	0	0.0
mean	371	$9.21 \cdot 10^{-6}$	2.4

overall gain: $(10000/371)/(5.75 \cdot 10^{-5}/0.92 \cdot 10^{-5}) = 4.3$

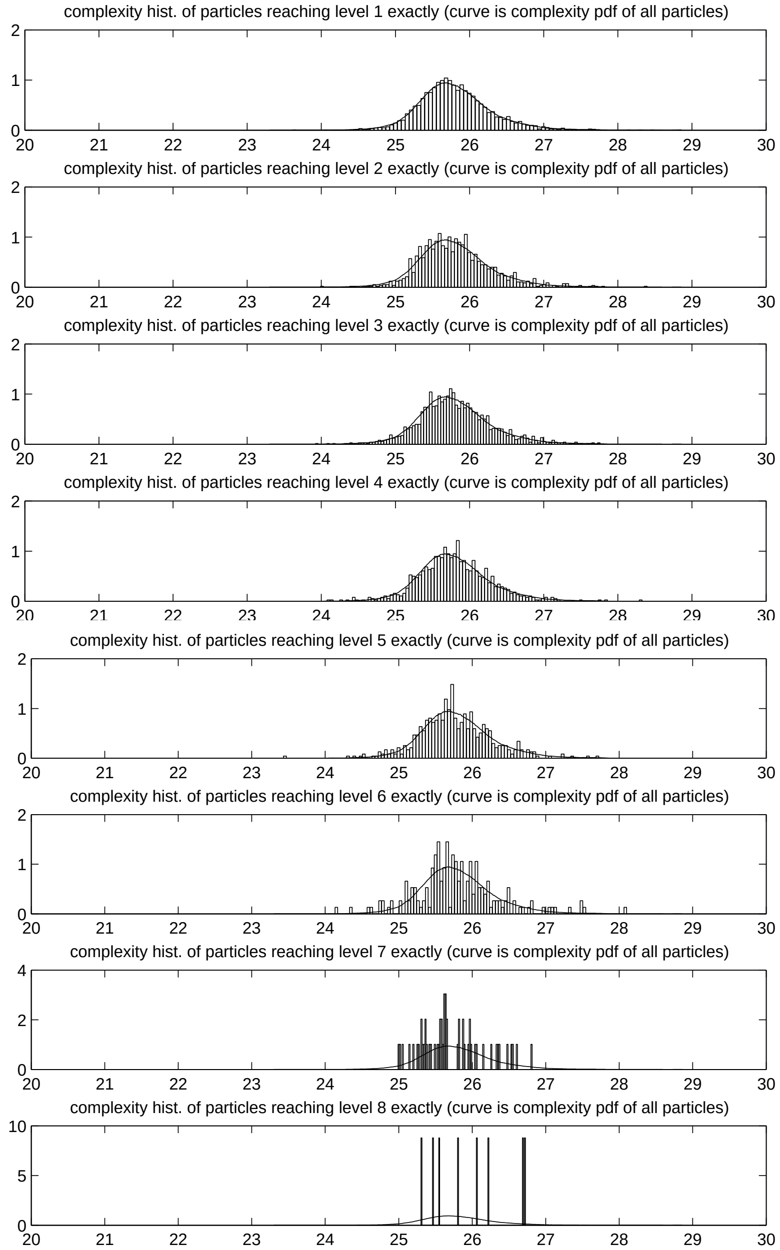

Figure 27: Histograms of complexity $M_{\max}$ for the particles hitting the conflict levels from 1 to 8 (run number 1).

Final outcome of the experiments

The speed-up factor obtained with the probabilistic approach in Section 5.1 was found to be one order of magnitude larger than that obtained with the geometric approach in Section 5.2. This means that the probabilistic complexity measure is more correlated with the collision risk than the geometric measure, and, as a consequence, it is more suitable for detecting those air traffic configurations that are difficult to control. A possible reason for this result is that the probabilistic complexity metric proposed in Section 5.1 strictly relates to the probability of conflict. Also, the geometric complexity metric proposed in Section 5.2 accounts for the flight speeds only indirectly, through the projected aircraft positions, which makes it difficult discriminating between collision and no collision situations.

6 Concluding remarks

In this final chapter we summarize the achievements realized within WP3.2, discuss their possible impact on the A^3 ConOps, and outline follow-up questions that calls for further investigation.

The approaches for complexity evaluation available in the literature were examined based on the features of a complexity metric that were found to be relevant to automated airborne self separation. A method that appeared portable to the A^3 ConOps was identified. A thorough analysis of this method led to the conclusion that some of its features hamper its applicability to the intended A^3 ConOps applications supporting strategic trajectory management and mid term conflict detection and resolution operations.

A probabilistic and a geometric approach to complexity evaluation were developed to better meet the challenges posed by the A^3 ConOps applications. Both approaches satisfy the feature relevant to airborne self separation. They both provide local measures of complexity that depend on the aircraft density and the traffic evolution, and not on the way the traffic is controlled. A key difference is that, whereas in the probabilistic approach the uncertainty affecting the aircraft predicted position is accounted for, in the geometric approach complexity is determined based on the nominal aircraft trajectories and neglecting uncertainty.

Since the goal of the geometric approach to complexity is to assess whether or not it would be convenient (from a tactical maneuvering perspective) for an aircraft to be at a specific position in a specific time, the corresponding metric is suitable for the A^3 ConOps application to trajectory management and, more specifically, for the identification of those complex areas that should better avoided in order to reduce the need for excessive tactical maneuvering.

Through a correlation analysis with collision risk, the probabilistic method was found to be better suited for supporting the ASAS mid term conflict detection and resolution operations by predicting those air traffic configurations that are difficult to control and may overload the ASAS CR module.

The two approaches could then be combined as follows. The geometric approach could be used to determine the complex areas-to-avoid, based on the aircraft RBTs available through SWIM. Areas-to-avoid will be computed on the ground and distributed onboard to support trajectory management operations. Complexity maps will be updated from time to time to take care of possible modifications of the aircraft RBTs. Unexpected deviations on a finer time scale will be accounted for by the probabilistic complexity metric tailored to a mid term time horizon. Appropriate joint tuning of design parameters and thresholds should be performed to optimize the overall complexity prediction functions within the A^3 ConOps.

Probabilistic complexity metrics could be used also for onboard trajectory design so as to preserve trajectory flexibility while optimizing performance. Interestingly, the level of flexibility of the designed trajectory can be tuned by modifying the level of uncertainty affecting the predicted aircraft future position. However, effective trajectory design algorithms should be conceived. In addition, at the current stage of development, the uncertainty affecting the aircraft future position is supposed to be uncorrelated, which may be a quite restrictive assumption. The case of correlated uncertainty requires investigation. Besides being more difficult from a modeling perspective since an appropriate spatial correlation structure has to be introduced (see e.g. [32]), the contribution to complexity of distinct aircraft will not be decoupled anymore but will have to be jointly evaluated, at least for aircraft within a sensible distance, where correlation is effective.

Apart from the weaknesses related to the individual approaches, some further weaknesses could emerge from the co-existence of the two methods. The analysis of this issue, however, goes far beyond the work plan in WP3.2.

References

[1] RTCA Task Force 3. Free flight implementation. Technical report, RTCA Inc., October 1995.

[2] S. Athénes, P. Averty, S. Puechmorel, D. Delahaye, and C. Collet. Complexity and controller workload: Trying to bridge the gap. In *International Conference on Human-Computer Interaction in Aeronautics, HCI-Aero*, Cambridge (MA), USA, 2002.

[3] A. Berlinet and C. Thomas-Agnan. *Reproducing kernel Hilbert spaces in probability and statistic*. Kluwer Academic Publisher, 2004.

[4] K. Bilimoria and M. Jastrzebski. Properties of aircraft clusters in the national airspace system. In *AIAA Aviation Technology, Integration and Operations Conference*, number AIAA 2006-7801, Wichita, Kansas, Sept. 2006.

[5] K. Bilimoria and H. Lee. Analysis of aircraft clusters to measure sector-independent airspace congestion. In *AIAA Aviation Technology, Integration and Operations Conference*, number AIAA 2005-7455, Arlington, VA, Sept. 2005.

[6] K.D. Bilimoria and M. Jastrzebski. Aircraft clustering based on airspace complexity. *7th AIAA Aviation Technology, Integration and Operations Conference*, 2007.

[7] Henk A.P. Blom, Jaroslav Krystul, G.J. (Bert) Bakker, Margriet B. Klompstra, and Bart Klein Obbink. Free flight collision risk estimation by sequential MC simulation. In C.G. Cassandras and J. Lygeros, editors, *Stochastic hybrid systems*, Automation and Control Engineering Series 24, pages 249–282. Taylor & Francis Group/CRC Press, 2007.

[8] Silvie Luisa Brázdilová, Petr Cásek, and Jan Kubalčík. Airspace complexity for airborne self separation. In *Proceedings of CEAS 2009 European Air and Space Conference*. Royal Aeronautical Society, 2009.

[9] Silvie Luisa Brázdilová, Petr Cásek, and Jan Kubalčík. Airspace complexity for airborne self separation. In *Proceedings of CEAS 2009 European Air and Space Conference*. Royal Aeronautical Society, 2009.

[10] E.P. Buckley, B.D. DeBaryshe, N. Hitchner, and P. Kohn. Methods and measurements in real-time air traffic control system simulation. Technical Report DOT/FAA/CT83/26, Federal Aviation Administration, Atlantic City, NJ, 1983.

[11] G. Chaloulos and J. Lygeros. Effect of wind correlation on aircraft conflict probability. *AIAA Journal of Guidance, Control, and Dynamics*, 30(6):1742–1752, 2007.

[12] A. Cloerec, K. Zeghal, and E. Hoffman. Traffic complexity analysis to evaluate the potential for limited delegation of separation assurance to the cockpit. In *18th Digital Avionics Systems Conference*, 1999.

[13] G. Cuevas, I. Echegoyen, J.G. Garca, P. Cásek, C. Keinrath, R. Weber, P. Gotthard, F. Bussink, and A. Luuk. Autonomous aircraft advanced (A^3) ConOps. iFly Deliverable 1.3, November 2008.

[14] D. Delahaye, P. Paimblanc, S. Puechmorel, J.M. Histon, and R.J. Hansman. A new air traffic complexity metric based on dynamical system modelization. In *21st Digital Avionics Systems Conference*, 2002.

[15] D. Delahaye and S. Puechmorel. Air traffic complexity: Towards intrinsic metrics. In *Proc. of the 3rd FAA/Eurocontrol ATM R&D Seminar*, Napoli, Italy, June 2000.

[16] D Delahaye and S Puechmorel. Air traffic complexity: Towards intrinsic metrics. In *Proceedings of the Second USA/EUROPE Air Traffic Management R&D Seminar*. Eurocontrol/FAA, 2000.

[17] D. Delahaye and S. Puechmorel. Air traffic complexity map based on nonlinear dynamical system. In *4th Eurocontrol Innovative Research Workshop & Exhibition*, 2005.

[18] D. Delahaye and S. Puechmorel. Air traffic complexity based on dynamical systems. In *CDC10*, pages 2069–2074, Atlanta, USA, December 2010.

[19] D. Delahaye, S. Puechmorel, R.J. Hansman, and J.M. Histon. Air traffic complexity based on nonlinear dynamical systems. In *5th USA/Europe Air Traffic Management R&D Seminar*, Budapest, Hungary, June 2003.

[20] R. Durrett. *Probability: theory and examples, Second edition.* Duxbury Press, 1996.

[21] H. Erzberger, R. A. Paielli, D. R. Isaacson, and M. M. Eshow. Conflict detection and resolution in the presence of prediction error. In *1st USA/Europe Air Traffic Management R&D Seminar, Saclay, France*, pages 17–20, 1997.

[22] H. Erzberger, R.A. Paielli, D.R. Isaacson, and M.M. Eshow. Conflict detection and resolution in the presence of prediction error. In *Proc. of the 1st USA/Europe Air Traffic Management R&D Seminar*, Saclay, France, June 1997.

[23] Chaboud et al. Air traffic complexity: Potential impacts on workload and cost. Technical Report EEC note 11/00, Eurocontrol, 2000.

[24] P. Flener, J. Pearson, M. Agren, C. Garcia-Avello1, M. Celiktin, and S. Dissing. Air-traffic complexity resolution in multi-sector planning using constraint programming. In *Air Traffic Management R&D Seminar*, 2007.

[25] G.H. Golub and C.F. Van Loan. *Matrix computations 2nd edition*. The Johns Hopkins University Press, 1989.

[26] G. Granger and N. Durand. A traffic complexity approach through cluster analysis. *5th USA/Europe Air Traffic Management R&D Seminar*, 2003.

[27] B. Hilburn. Cognitive complexity in air traffic control: A literature review. Technical Report 04/04, EUROCONTROL, 2004.

[28] J. Histon, G. Aigoin, D. Delahaye, R.J. Hansman, and S. Puechmorel. Introducing structural considerations into complexity metrics. In Eurocontrol-FAA, editor, *Fourth USA/EUROPE ATM R& D Seminar*, 2001.

[29] J. Histon, R.J. Hansman, G. Gottlieb, H. Kleinwaks, S. Yenson, D. Delahaye, and S. Puechmorel. Structural considerations and cognitive complexity in air traffic control. In IEEE-AIAA, editor, *21st Air Traffic Management for Commercial and Military Systems*, 2002.

[30] J. Hu. A study of conflict detection and resolution in free flight. Master's thesis, Department of Electrical Engineering and Computer Sciences, University of California at Berkeley, 1999.

[31] J. Hu, M. Prandini, and S. Sastry. Aircraft conflict prediction in presence of a spatially correlated wind field. *IEEE Transactions on Intelligent Transportation Systems*, 6(3):326–340, 2005.

[32] J. Hu, M. Prandini, and S. Sastry. Aircraft conflict prediction in the presence of a spatially correlated wind field. *IEEE Transactions on Intelligent Transportation Systems*, 3:326–340, 2005.

[33] H. Idris, R. Vivona, and J-L Garcia-Chico. Trajectory-oriented approach to managing traffic complexity – operational concept and preliminary metrics definition. Ames Contract NNA07BB26C NASA/CR-2008-215121, National Aeronautics and Space Administration, Langley Research Center, Hampton, Virginia, 2008.

[34] H. Idris, R. Vivona, J-L Garcia-Chico, and D. Wing. Distributed traffic complexity management by preserving trajectory flexibility. *26th IEEE/AIAA Digital Avionics Systems Conference*, 2007.

[35] H. Idris, D. Wing, R. Vivona, and J-L Garcia-Chico. A distributed trajectory-oriented approach to managing traffic complexity. In *7th AIAA Aviation Technology, Integration and Operations Conference*, number AIAA 2007-7731, Belfast, Northern Ireland, Sept. 2007.

[36] Wyndemere Inc. An evaluation of air traffic control complexity. Technical Report Contract NAS2-14284, October 1996. Final Report.

[37] M.A. Ishutkina, E. Feron, and K.D. Bilimoria. Describing air traffic complexity using mathematical programming. In *AIAA 5th Aviation, Technology, Integration, and Operations Conference*, 2005.

[38] T.M. Janaki, G. Rangarajan, S. Habib, and D. Ryne. Computation of the lyapunov spectrum for continuous-timpe dynamical systems and discrete maps. *Physical Review*, 60(6), 1999.

[39] P. Kopardekar. Dynamic density: A review of proposed variables. Technical report, FAA, 2000. FAA NAS Advanced Concepts Branch ACT-540.

[40] P. Kopardekar and S. Magyarits. Dynamic density: Measuring and predicting sector complexity. In *21st Digital Avionics Systems Conference (DASC)*, Irvine, California, 2002.

[41] B. Kriwan, R. Scaife, and R. Kennedy. Investigating complexity factors in UK air traffic management. In *Human Factors and Aerospace Safety*, 2001.

[42] I.V Laudeman, S.G Shelden, R Branstrom, and C.L Brasil. Dynamic density: an air traffic management metric. Technical report, NASA TM-1998-112226, 1998.

[43] I.V. Laudeman, S.G. Shelden, R. Branstrom, and C.L. Brasil. Dynamic density: An air traffic management metric. Technical Report TM-1998-112226, NASA, 1998.

[44] A. Lecchini, W. Glover, J. Lygeros, and J. Maciejowski. Monte Carlo optimization for conflict resolution in air traffic control. In H.A.P. Blom and J. Lygeros, editors, *Stochastic Hybrid Systems: Theory and Safety Critical Applications*, volume 337, pages 257–276. Springer Berlin, 2006.

[45] K. Lee, E. Feron, and A. Pritchett. Air traffic complexity: An input-output approach. In *Air Traffic Management R&D Seminar*, 2007.

[46] K. Lee, E. Feron, and A. Pritchett. Air traffic complexity: An input-output approach. In *American Control Conference*, New York City, USA, July 2007.

[47] K. Lee, E. Feron, and A. Pritchett. Describing airspace complexity: Airspace response to disturbances. *Journal of Guidance, Control, and Dynamics*, 32(1):210–222, January-February 2009.

[48] A. Majumdar and W.Y. Ochieng. The factors affecting air traffic controller workload: a multivariate analysis based upon simulation modelling of controller workload. Technical report, Centre for Transport Studies, Imperial College, London, 2000.

[49] A. Masalonis, M. Callaham, Y. Figueroa, and C. Wanke. Indicators of airspace complexity for traffic flow management decision support. In *12th International Symposium on Aviation Psychology*, Dayton, Ohio, 2003.

[50] A.J. Masalonis, M.B. Callaham, and C.R. Wanke. Dynamic density and complexity metrics for realtime traffic flow management. In *5th USA/Europe Air Traffic Management Seminar*, Budapest, Hungary, 2003.

[51] R.H. Mogford, J.A. Guttman, S.L. Morrow, and P. Kopardekar. The complexity construct in air traffic control: A review and synthesis of the literature. Technical Report DOT/FAA/-CT TN95/22, FAA, Atlantic City, NJ, 1995.

[52] S. Mondoloni and D. Liang. Airspace fractal dimension and applications. In Eurocontrol-FAA, editor, *Fourth USA/EUROPE Air Traffic Management R& D Seminar*, 2001.

[53] B. Klein Obbink. MFF airborne self separation assurance OSED, Report MFF R733D. Available at http://www.medff.it/public/index.asp, April 2005.

[54] R. A. Paielli and H. Erzberger. Conflict probability estimation for free flight. *Journal of Guidance, Control, and Dynamics*, 20(3):588–596, 1997.

[55] R.A. Paielli and H. Erzberger. Conflict probability estimation for free flight. *Journal of Guidance, Control, and Dynamics*, 20(3):588–596, 1997.

[56] M. Prandini, J. Hu, J. Lygeros, and S. Sastry. A probabilistic approach to aircraft conflict detection. *IEEE Transactions on Intelligent Transportation Systems*, 1(4):199–220, 2000.

[57] M. Prandini, J. Hu, J. Lygeros, and S. Sastry. A probabilistic approach to aircraft conflict detection. *IEEE Transactions on Intelligent Transportation Systems, Special Issue on Air Traffic Control - Part I*, 1(4):199–220, 2000.

[58] M. Prandini, L. Piroddi, S. Puechmorel, and S.L. Brázdilová. Complexity metrics applicable to autonomous aircraft. iFly Deliverable 3.1, January 2009.

[59] M. Prandini, L. Piroddi, S. Puechmorel, and S.L. Brázdilová. Toward air traffic complexity assessment in new generation air traffic management systems. *IEEE Trans. on Intelligent Transportation Systems*, 2011. To appear.

[60] M. Prandini, V. Putta, and J. Hu. A probabilistic measure of air traffic complexity in three-dimensional airspace. *International Journal of Adaptive Control and Signal Processing, special issue on Air Traffic Management: Challenges and opportunities for advanced control*, pages 1–16, 2010. To appear.

[61] Maria Prandini, Henk A.P. Blom, and Bert (G.J.) Bakker. Interim report on importance sampling of multiple aircraft encounter geometries. iFly Deliverable 7.2c, September 2010.

[62] INTENT project. Deliverable 2-1 – capacity. http://www.intentproject.org/, 2002.

[63] S. Puechmorel and D. Delahaye. New trends in air traffic complexity. In *ENRI International Workshop on ATM/CNS (EIWAC 2009)*, Tokyo, Japan, March 2009.

[64] M.D. Rodgers, R.H. Mogford, and L.S. Mogford. The relationship of sector characteristics to operational errors. Technical Report DOT/FAA/AM-98/14, FAA, Washington DC, 1998.

[65] B Sridhar, K.S Seth, and S Grabbe. Airspace complexity and its application in air traffic management. In *Proceedings of the Second USA/EUROPE Air Traffic Management R&D Seminar*. Eurocontrol/FAA, 2001.

[66] B. Sridhar, K.S. Sheth, and S. Grabbe. Airspace complexity and its application in air traffic management. In *Proc. of the 2nd USA/Europe Air Traffic Management R&D Seminar*, Orlando, USA, Dec. 1998.